August 2016

The Study of Locating Ground Faults in DC Microgrid Using Wavelet Transform

Ruijing Yang
University of Wisconsin-Milwaukee

THE STUDY OF LOCATING GROUND FAULTS IN DC MICROGRID USING WAVELET TRANSFORM

by

Ruijing Yang

A Thesis Submitted in

Partial Fulfillment of the

Requirements for the Degree of

Master of Science

in Engineering

at

The University of Wisconsin-Milwaukee

August 2016

ABSTRACT

THE STUDY OF LOCATING GROUND FAULTS IN DC MICROGRID USING WAVELET TRANSFORM

by

Ruijing Yang

The University of Wisconsin-Milwaukee, 2016
Under the Supervision of Professor Robert M. Cuzner

As the proliferations of distributed generation and power electronic equipment in power systems, direct current (DC) microgrid emerged and attracted more and more researchers' attentions. Protection of DC microgrid is a big challenge and to build a well-function protection system, locating the faults accurately is a critical issue. It is easy to find the location of short circuit faults in DC microgrid. However, it is difficult to locate ground faults in DC microgrid because of the spray capacitors and the large amount of distributed resources.

In this thesis, Wavelet Transform is applied to decompose the common mode currents that is collected at different sensor points in a DC microgrid and capture the characterization of every single ground fault. And based on these characterizations, a single ground fault location algorithm is proposed.

MATLAB/Simulink and PLECS are used to assist in the process. Simulink is used to build the three phase source feeding the DC microgrid and PLECS is used to build the model of

DC microgrid and measure the common mode current at different sensor points when a single ground fault is applied.

TABLE OF CONTENTS

LIST OF FIGURES

LIST OF TABLES

ACKNOWLEDGEMENTS

First of all, I would like to express my heartfelt gratitude to my advisor Professor Robert M. Cuzner for his patient guidance. I sincerely appreciate for all those discussions and conversations in which Professor Cuzner shared his invaluable knowledge and experience, and helped me to work out difficulties. I feel so lucky and blessed to have such a great advisor who spares no effort to help students. I would like to specifically thank Professor David C. Yu, for his support and encouragement to me, and for his effort to build up the cooperative relationship between University of Wisconsin-Milwaukee and the universities in China, which provide opportunities to students like me to study here.

Additionally, I want to thank my friends for their advice in my work and help in my life, especially thank Qianqian for her help both in my study and personal life.

Finally, I would like to express my deepest appreciation to my family, for their unconditional love and support, only with their love I can go so far to know more about the wonderful world.

Chapter 1 Introduction

In this chapter, the background, research status and research objective are presented.

1.1 Background

In this section, the concept of DC microgrid will be briefly introduced and the deficiency of Fourier Transformation will also be explained.

1.1.1 DC Microgrid

Nowadays, society relies more and more on electricity so that the demand for undisturbed electricity is growing. Under this circumstance, the outages would have worse effects on the customers and the loss of outages would also increase. [1] Meanwhile, with climate change weather impacts to the grid are occurring at an increasing rate. To overcome these challenges, a more reliable network is required. With the development of renewable energy sources, such as photovoltaic (PV) plant and full-converter wind power plant, the distributed resources have gradually infiltrated into the electric power system.

A part of the distribution system with its sources and loads can form an isolated electric power system—a microgrid. [2] The microgrid is connected to grid and under the normal operating mode, the demand of loads is met by local sources and, if necessary, also by the automotive current (AC) grid. When an AC grid outage occurs, the operating mode of microgrid would be changed into island mode, and then instead of facing the outage, the loads would be met by the distributed resources and energy storage system in the microgrid.

Due to this high reliability and high flexibility, the microgrid is well suited to protecting sensitive loads from power outages and disturbances. [3]

Among all kinds of microgrid, a DC microgrid is most suitable to use where most of the loads are sensitive electronic equipment. [4] An example of a small DC microgrid is shown in Figure 1-1. AC microgrids are much more common than DC microgrids because AC systems can rely upon the existing electrical distribution infrastructure and proven principles and hardware components to ensure reliability. However, the technical and economic developments during last decades have established the opportunity to create a new competitive microgrid system based on modern power electronic technology. Compared with a AC microgrid, the loads, sources and energy storage system can be connected through simpler and more efficient power-electronic interfaces in a DC microgrid. More importantly, the use of DC in end-user appliances used in households and office buildings, such as laptops, air conditioners and microwave ovens is increasing. Thus, DC microgrids are becoming more and more common now.

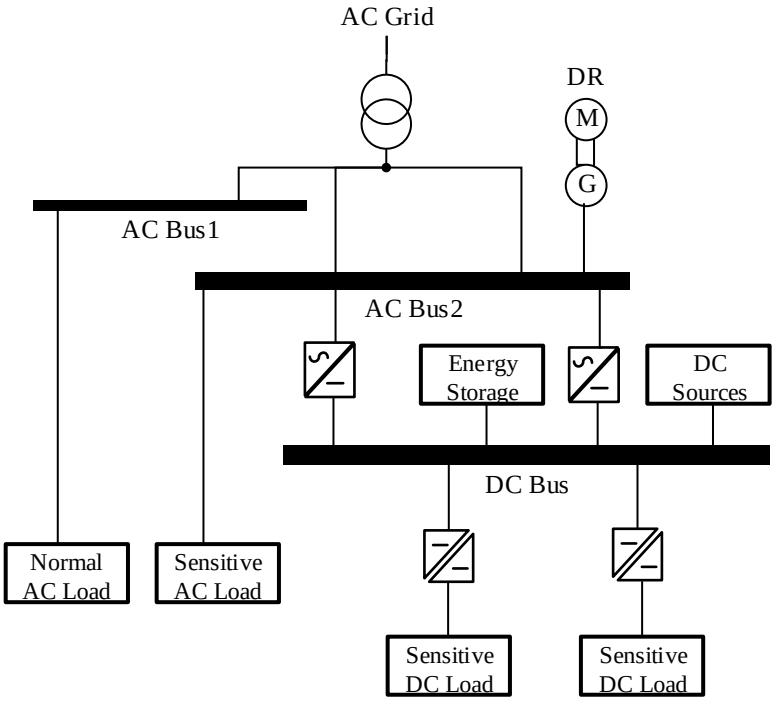

Figure 1-1 Example of a small DC microgrid

Because multiple power sources are involved into the DC microgrid and faults are of the most potential to cause indirect contact risk, to ensure reliable operation of DC microgrid, it is important to have a well-function protection system which can eliminate or isolate the faults from healthy parts quickly and accurately. To design a protection system like this, first and foremost, the faults must be located quickly and accurately.

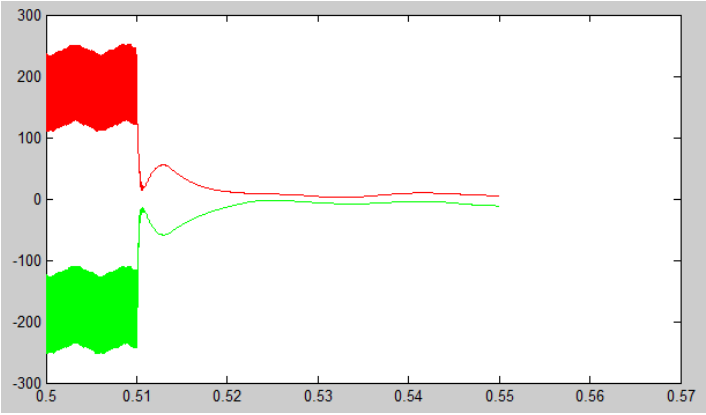

Figure 1-2 Variation of pole-to-ground voltages (a short circuit fault)

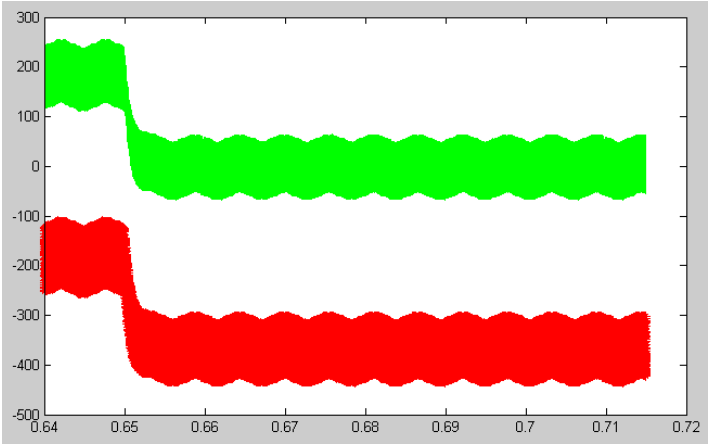

Figure 1-3 Variation of pole-to-ground voltages (a ground fault)

Figure 1-2 shows the variation of pole-to-ground voltages when a short circuit fault happens. Since the microgrid cannot keep working under this situation, it is easy to find where the fault is. Figure 1-3 shows the variation of pole-to-ground voltages when a ground circuit fault happens. Compared with previous case, both of the pole-to-ground voltages will have a shift but the differential voltage at load does not change significantly, which means the microgrid can still keep working. In this case, the ground fault may not need to be isolated, but still need to be located. However, due to the stray capacity between cables and ground and the multiple power sources in DC microgrid, the paths of ground fault currents would be complicated, which results in the difficulty of locating the fault. As the transient status of the system after the fault occurs consists of a large amount of information, to locate the fault accurately, it would be helpful if the transient signals caused by ground faults could be collected and an appropriate tool could be found to capture the characteristics of transient status.

1.1.2 Deficiency of Fourier Transformation

Fourier Transformation (FT) is the most popular tool used to analyze signals. However, because of its deficiency, FT does not perform very well when it is used to analyze the

nonstationary signals. Applying FT to decompose nonstationary signals can still help researchers know how many kinds of frequency components are in the signals and the corresponding amplitudes of those frequency components, but it cannot help researchers know the time when the specific frequency occurs. In other words, the time variable of original signals is eliminated in the decomposition results. To overcome this deficiency, Short-time FT was proposed and its basic principle is dividing a long time signal into many short segments that have equal length and then computing each short segment separately with the Fourier Transformation. Applying Short-time FT to analyze nonstationary signals usually can get good results. However, the length of the window of Short-time FT is fixed, which means if the length of the window is too narrow, the decomposition results in frequency-domain might not be accurate enough, while if the length of the window is too wide, the decomposition results in time-domain might not be accurate enough.

Given the deficiency of FT, in this thesis, Wavelet Transform (WT) is chosen as the tool to decompose and analyze the transient signals caused by the single ground fault. Compared with FT, WT has some significant advantages. The first advantage is that the time variable is kept in the decomposition results of WT. The second advantage is that the sub signals in every frequency sub-band can be reconstructed so that the relationship between time, signal and frequency can be found. In this thesis, this advantage can help to find the characteristics of signals caused by single ground fault. The third advantage is as a general rule, a narrower window is needed when decomposing the high frequency signal and a wider window is needed when decomposing the low frequency signals. Different from the fixed window in FT, WT can adjust the width of window automatically because

it uses a time-scale region and changes the transform basis from infinite trigonometric function basis into finite attenuate wavelet basis. Given these advantages, WT is chosen as the tool to analyze the signals in this paper and the basic principles of WT will be introduced in detail in Chapter 3.

1.2 Research Status

As a powerful analyzing tool, WT has been applied to locating ground faults occurring not only in high voltage power system, but also in distribution network in the reported research [5] - [18]. General approaches are decomposing the original signals by WT and capturing the characteristics of original signals. These characteristics will be regarded as characteristic variables and put into some algorithms such as artificial neural network and differential evolution algorithm. There are some different ways to capture these characteristics of original signals. One of the commonly used ways is calculating the energy of coefficients in sub-bands according to Parseval's theorem. Reference [5] - [12] are the representatives of this kind of method. This method is based on the energy theory that the fault waveform in any signal can be considered as a result of change in the energy status of that signal. [8] The energy distribution of the voltage and current transient signal in the scale space reflect their energy distribution in frequency domain. [13] Thus, the energy characteristic of sub-bands can be used to identify the place where the fault happens.

Another way to capture the characteristics is calculating the wavelet singular entropy (WSE). This method is also based on the energy theory. Compared to previous method, calculating WSE is much more complicated but it is more sensitive to the transient

variation produced by the faults. Higher WSE implies more complex interactions in different frequency signal components so that it can be used to indicate the uncertainty of the energy distribution in the time-frequency domain with a high immunity to noise. Reference [13] - [15] are the representatives of this kind of method.

Besides these two methods, the protection algorithm proposed in reference [16] uses WT to decompose the transient signal and locate the fault by comparing the maximum value of coefficients. Reference [17] puts the different signals under the same frequency range, then decomposes them by WT and compares the results to locate the fault. Reference [18] focuses on the high impedance ground faults and WT is applied to filter out some harmonics under specific frequency range. Then the root mean square (RMS) value of harmonics are calculated by using the wavelet coefficients directly and the fault is identified by compare the variation of RMS difference.

1.3 Research Objective and Article Layout

The main objective of this thesis is using WT to decompose and capture the characteristics of common mode (CM) currents measured at different sensor points after a single ground fault happens in the DC microgrid. And then proposing a location algorithm based on those characteristics, to distinguish all the kinds of single ground faults that occur in DC microgrid.

There are 5 chapters in this thesis. Chapter 1 briefly introduces the background of this research and the research status of this area. Research objective and article layout are also

included in this chapter. Chapter 2 mainly discusses the characteristics of the DC microgrid built in this research. Equivalent circuit of CM current is also shown in this chapter. Chapter 3 mainly explains the basic principle of WT. Chapter 4 is mainly composed of simulation part and analysis part. Firstly, the paths of grounding current and characteristics of every single ground fault are presented. Then these characteristics are summarized and the location algorithm is proposed. Finally, Chapter 5 presents the conclusion and prospects the future work.

Chapter 2 Description of the DC Microgrid

This section covers the characteristics and the equivalent circuit of CM current of the DC microgrid built in this research.

2.1 Characteristics of DC Microgrid Model

In this thesis, a DC microgrid is built as the base to analyze the characteristics of different kinds of ground faults, in which there are is Hub connected with transformer/rectifier and DC bus, two Garages where there are PV panels and three Houses acting as the DC loads. The whole view of the DC microgrid used in this thesis is shown in Figure 2-1.

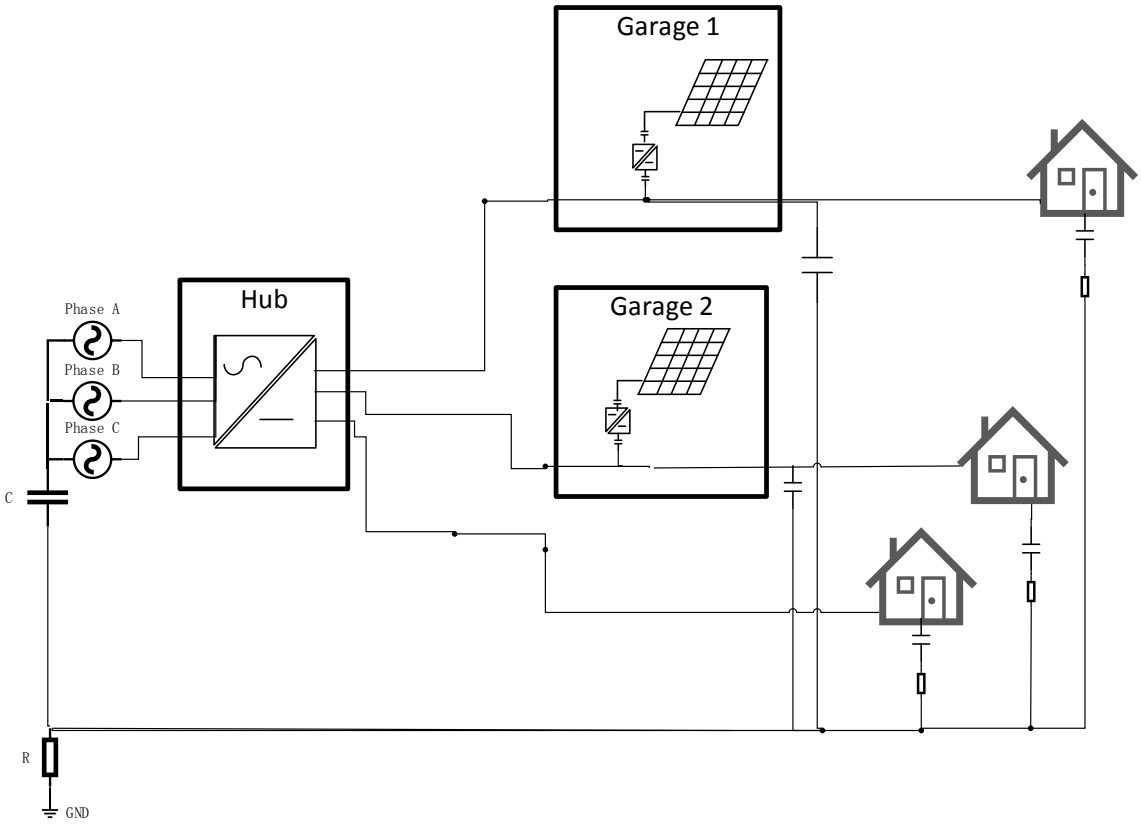

Figure 2-1 The whole view of the DC microgrid

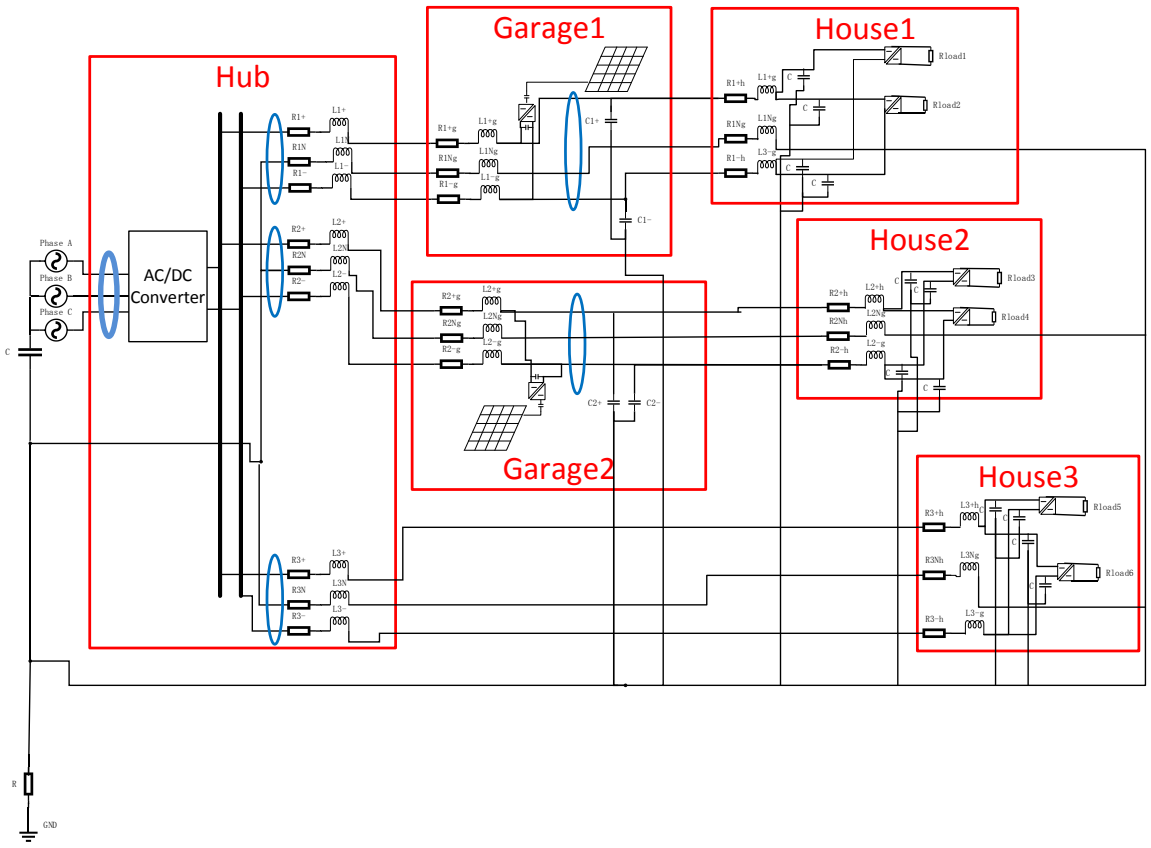

Figure 2-2 The structure of the DC microgrid

The structure of the DC microgrid is shown in detail in Figure 2-2. In general, DC microgrid can be ungrounded, high resistance grounded, or floating grounded. And based on different grounding types, DC microgrid shows different behavior when the single ground fault occurs. The microgrid used in this thesis is unipolar and has one voltage level to which all the loads in this microgrid are connected. The neutral point of the transformer is connected to ground through a capacitor and a resistance and the neutral pole of DC system is connected to ground through the same resistance. Under this grounding way, the DC pole-to-ground voltages would remain constant at $\pm V_{DC}/2$ value. [19] So assuming the ground fault happens in the DC system, the positive pole-to-ground voltage will shift to $+V_{DC}$ value while the negative pole-to-ground voltage will become zero when the ground fault happens at the negative pole. And the negative pole-to-ground voltage will shift to −

V_{DC} value while the positive pole-to-ground voltage will become zero when the ground fault happens at the positive pole. On the other hand, if the ground fault happens in the AC system, the resultant voltage to ground shift will reflect back into the rest of the system by the same principle that was applied to ground faults at the main DC distribution bus and all the voltage interfaces will shift by $\pm V_{DC}$ value. [20] To capture the characteristics easily, bigger currents are expected. Thus, in this thesis, the grounding type of this DC microgrid is floating grounding and the value of the resistance to a common equipotential surface is 20 Ohms.

There are some other important things needed to be pointed out. The first thing is the existence of PV panels. Under the normal operating mode, the PV panels is used to feed the loads as the local sources. However, when a single ground fault occurs, PV panels and their related electronic converters will affect the system in different ways depending on the grounding of the system. [21] In the system is ungrounded (floating), if the single ground fault occurs at one feeder, the PV panels connected to this unhealthy feeder may not only feed the loads connected to this feeder, but also feed the ground fault. Meanwhile, the PV panels connected to the healthy feeder may also make contributions to the grounding current. In this model, there are two PV panels which are connected to the Feeder 1 and Feeder 2 separately through DC/DC converters, but because the system is floating, they do not make any contributions to the fault current.

The second thing is the stray capacitance. Because of the using of low voltage (LV) cables and EMI filters connected to the inputs of the loads, the stray capacitance between cables

and ground cannot be ignored, which exists in the two Garages and three Houses. When a single ground fault happens, the pole-to-ground voltages of unhealthy feeder will have a shift and the pole-to-ground voltages of healthy feeders will also have a transient status, which means there would be transient currents flowing through these stray capacitors. Since the path of these transient currents depends on the location of ground faults and these transient currents will affect the CM currents measured, this could be one of the characteristics that can help to locate the ground fault.

The third thing is that the length of cables used in Garage 1 and Garage 2 are different. The cables used in Garage 1 is 1000 feet long while the cables used in Garage 2 is 500 feet long, which will result in the different characteristics such as amplitudes shown in the sub-bands because longer cable will bring more low frequency components into the signal. So in general, the amplitude of the low frequency components in the signal collected near Garage 1 might be higher than that in the signal collected near Garage 2.

The last but not least is about the sensor points. There are six sensor points measuring the CM current in this microgrid. The first one is located before the AC/DC converter and it is used to measure the sum of current coming from phase A, B and C. The second to fourth sensor points are located near Hub and they are used to measure the CM current of three feeders respectively. The currents measured by these three sensors are called Icm1, Icm2 and Icm3 respectively. The fifth and sixth sensor points are located near the two Garages respectively and they are measuring the CM current flowing through the Feeder 1 and Feeder 2 after the PV panels. The currents measured by these two sensors are called Igcm1

and Igcm2 respectively. The reason why the CM currents are measured will be explained in Section 2.3.

2.2 Circuit of Ground Fault

The circuit of the ground fault applied in this thesis is shown in Figure 2-3.

Figure 2-3 The circuit of ground fault

Based on the location of the ground fault, it can be divided into single phase-to-ground fault that occurs at the AC side and single pole-to-ground fault that occurs at the DC side. In this thesis, the grounding resistance in all kinds of ground fault is set up as 20 Ohms.

2.3 Equivalent Circuit of Common Mode Current

Two modes of circuit operation are normally distinguished: differential mode (DM) and CM. The DM is the desired operation of a circuit. The CM (sometimes used with other similar quantities such as the zero-sequence current or neutral-point voltages) in contrast is the unintended operation of a circuit, often the result of environmental interference, asymmetric design, or parasitic couplings. [22] In the case that power system has a single ground fault, no matter where the fault is, the system will become unbalanced and asymmetric, which results in a big change of CM variables. In other word, CM variables can be regarded as the symptom to show the variations of the system. Given this reason, the original signals which is used to analyze are the CM currents measured at different sensor points.

CM current and CM voltage in Figure 2-4 are defined as: [22]

$$i_{CM} = i_1 + i_2 \qquad \text{Equation 2-1}$$

$$v_{CM} = \frac{v_{1P} + v_{2P}}{2} \qquad \text{Equation 2-2}$$

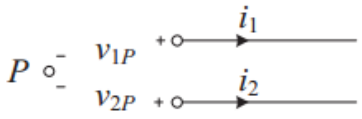

Figure 2-4 Diagram for CM and DM definitions

Reference [22] - [24] propose some rules that can be used to transform the DM circuit into their equivalent CM circuit during the single ground fault. And since PV panels do not make any contributions to the fault current, the equivalent CM circuits of PV panels are not required. The equivalent CM circuit of the model is shown in Figure 2-5 and the basic components are already marked.

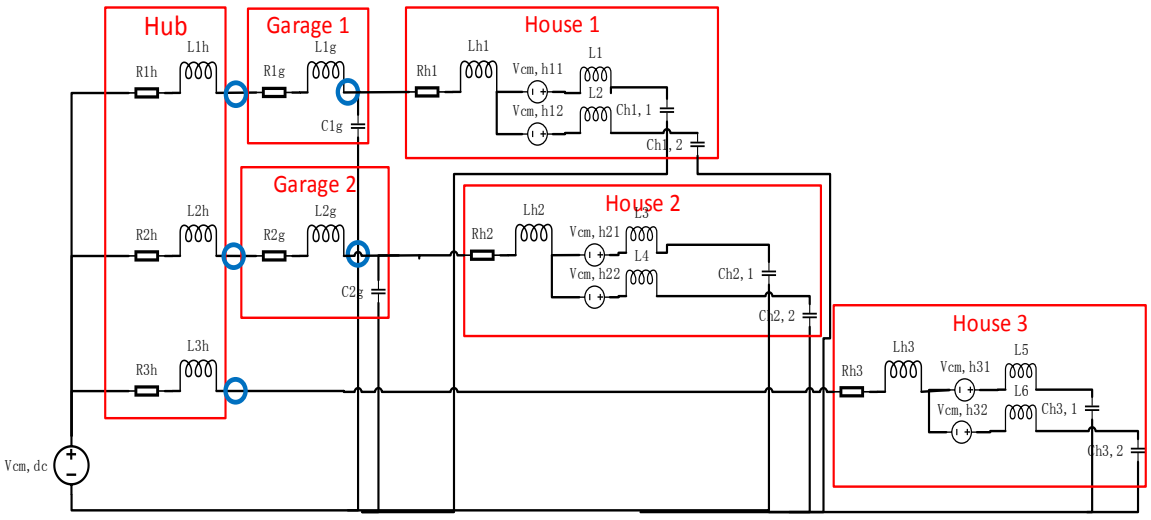

Figure 2-5 The equivalent CM circuit of the model

The values of every element in this CM circuit are shown in the Table 2-1.

Table 2-1 Equivalent CM circuit characteristic data

Elements	Values

R_{1h}&R_{2h}&R_{3h}	0.0005Ω
L_{1h}&L_{2h}&L_{3h}	1μH
R_{1g}	0.1Ω
L_{1g}	0.5μH
R_{2g}	0.05Ω
L_{2g}	0.25μH
C_{1g}&C_{2g}	2μF
L_1&L_2	90μF
L_3&L_4	90μF
L_5&L_6	90μF
$C_{h1,1}$&$C_{h1,2}$	2μF
$C_{h2,1}$&$C_{h2,2}$	2μF
$C_{h3,1}$&$C_{h3,2}$	2μF
R_{h1}&R_{h1}&R_{h1}	0.0005Ω
L_{h1}&L_{h2}&L_{h3}	1μH
Common mode voltage of DC bus $V_{cm,dc}$	190V
Common mode voltage of 1st load in House 1 $V_{cm,h11}$	-121V
Common mode voltage of 2nd load in House 1 $V_{cm,h12}$	-103.5V
Common mode voltage of 1st load in House 2 $V_{cm,h21}$	-121V
Common mode voltage of 2nd load in House 2 $V_{cm,h22}$	-103.5V
Common mode voltage of 1st load in House 3 $V_{cm,h31}$	-121V
Common mode voltage of 2nd load in House 3 $V_{cm,h32}$	-103.5V

Chapter 3 Wavelet Transform

This section covers the basic principles of wavelet transform.

3.1 Definition of Wavelet Function

Here is the basic principle of WT. The analyzed signal is decomposed into different scales using a wavelet analyzing function called 'mother wavelet' or 'wavelet function' and this wavelet is scaled and translated to match an input signal locally.[16] If the FT function of a function $\psi(t)$ can be described as $\hat{\psi}(\omega)$ and it matches the Equation 3-1 as follow in the function space $L^2(R)$, then the function $\psi(t)$ is a mother wavelet. [22]

$$C_\psi = \int_{-\infty}^{+\infty} |\omega|^{-1} \left| \hat{\psi}(\omega) \right|^2 d\omega < +\infty \qquad \text{Equation 3-1}$$

WT is characterized by a translation parameter *b* and a dilation parameter *a*. The dilation parameter *a* determines the size of the window in which the WT is performed and the translation parameter *b* determines the time corresponding to the center point of each window. For each 'mother wavelet' $\psi(t)$, a family can be obtained by scaling $\psi(t)$ by *a* and translation of $\psi(t)$ by *b*: [26]

$$\psi_{a,b}(t) = \frac{1}{\sqrt{a}} \psi\left(\frac{t-b}{a}\right) \qquad \text{Equation 3-2}$$

3.2 Characteristics of Wavelet Transform

In general, two types of wavelet transforms can be distinguished, namely the Continuous Wavelet Transform (CWT) and the Discrete Wavelet Transform (DWT).

3.2.1 Continuous Wavelet Transform

The CWT of a signal $f(t)$ at time *b* and scale *a* is calculated by Equation 3-3 as follow with $\psi(t)^*$, which is the complex conjugated of the wavelet function $\psi(t)$: [27]

$$WT(a,b) = \int_{-\infty}^{\infty} f(t) \frac{1}{\sqrt{a}} \psi^*(\frac{t-b}{a}) dt \qquad \text{Equation 3-3}$$

3.2.2 Discrete Wavelet Transform

If the dilation parameter *a* and the translation parameter *b* in Equation 3-2 can be described as $a=a_0{}^j$ and $b=ka_0{}^j b_0$, then the discrete wavelet function can be described as follow:

$$\psi_{j,k}(t) = \frac{1}{\sqrt{a_0^j}} \psi(\frac{t}{a_0^j} - kb_0) \qquad \text{Equation 3-4}$$

In which a_0 is the scale factor and bigger than one, b_0 is the shifting factor, and *j* is integer. Based on Equation 3-4, the basic principle of DWT can be explained through the Equation 3-5: [28]

$$C_{j,k} = \int_{-\infty}^{\infty} f(t) \psi_{j,k}^* dt = \left\langle f, \psi_{j,k} \right\rangle \qquad \text{Equation 3-5}$$

Where $C_{j,k}$ is the wavelet coefficient that represents the correlation between the (scaled) wavelet and the original signal. [16] Wavelet coefficients is the most commonly used object of study in previous references to capture the characteristics of original signals. However, in this thesis, wavelet coefficients are not the study subject. The sub signals reconstructed from wavelet coefficients are the study subject. The decomposed sub signal in every sub-band can be achieved by Equation 3-6, which is the reconstruction formula:

$$f(t) = C \sum_{-\infty}^{\infty} \sum_{-\infty}^{\infty} C_{j,k} \psi_{j,k}(t) \qquad \text{Equation 3-6}$$

Where *C* is a signal-independent constant.

CWT is the convolution of the signal multiplied by scaled and shifted versions of the mother wavelet. This continuous process results in many wavelet coefficients and a long calculation process. [16] Given that a fast processing algorithm is required in fault detection applications, in this thesis, DWT is chosen to be the tool to analyze the common mode currents.

3.3 Mallat Algorithm

There are several implementation methods of DWT. The oldest and most famous one is the Mallat pyramidal algorithm. In 1986, based on the previous studies, Mallat and Meyer proposed Multiresolution Analysis (MRA) and explained the multiresolution characteristics of wavelets. Then in 1988, Mallat and Meyer combined multiresolution analysis with digital filtering theory and then produced Mallat algorithm, a fast wavelet decomposition and reconstruction algorithm.

Mallat algorithm is a fast tower structure algorithm based on orthonormal wavelet transform. The schematic diagram of the Mallat decomposition algorithm is shown in Figure 3-1. [29]

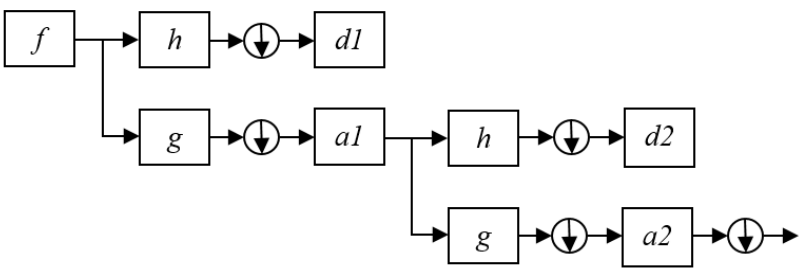

Figure 3-1 Schematic diagram of the Mallat decomposition algorithm

The original signal represented by *f* is decomposed by passing through a low-pass filter represented by *g* and a high-pass filter represented by *h* simultaneously. The output of the high-pass filter is called detail coefficients represented by *d* while the output of the low-pass filter is called approximation coefficients represented by *a*. *d*1 and *a*1 represents the detail coefficients and the approximation coefficients at the first level respectively, and *d*2 and *a*2 represents the detail coefficients and the approximation coefficients at the second level respectively. This decomposition would repeat itself until meeting the requirements of levels. Due to this decomposition process, the input signal must be divided into *n*+1 sub-bands where *n* is the number of levels. Based on the frequency of original signal, the frequency ranges of the sub-bands after three levels decomposing are presented in Figure 3-2.

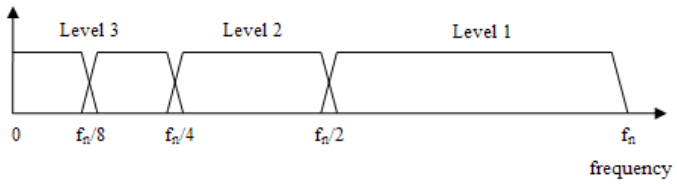

Figure 3-2 Frequency ranges of DWT decomposition results

3.4 Daubechies Wavelets

In DWT, the main characteristics of wavelet base functions contain compactly supported length, filter length, symmetry, extinction moment order and regularity. [16] Based on these characteristics, there are many kinds of wavelet base functions which can be used in analyzing the signals caused by fault. Which wavelet base function is the most proper one depends on the characteristics of the original signals. In this thesis, Daubechies (Db) Wavelets is chosen.

Db Wavelets are a family of orthogonal wavelets and defined by computing running averages and differences via scalar products with scaling signals and wavelets. For the Db WT, the scaling signals and wavelets have slightly longer supports than other kinds of wavelet base functions, which provides a tremendous improvement in the capabilities and results in the good performing in noise removal and signal recognition. As a general rule, when analyzing the signals coming from power system, given that these signals usually contain a large amount of transient components, Db Wavelets are the most suitable wavelet base function for the multiband analysis. That is why the Db Wavelets are chosen to be the tool in this thesis.

After selecting the wavelet base function, there are two parameters need to be selected. The first one is the N of DbN. Db1 - Db10 are the most commonly used among DbN series wavelet. The chosen of N not only depends on the characteristics of original signals, but also needs to take consideration of the main characteristics of Db Wavelets. The most obvious differences among DbN series wavelet are the length of the supports of their scaling signals and wavelets. Compactly supported length and filtering length of DbN series wavelet are both 2N, while the extinction moment order is N. [16] The extinction moment order limits the ability of wavelets to represent polynomial behavior or information in a signal. The extinction moment order is bigger, which means the N is bigger, the Db WT produces smaller size fluctuation values. Meanwhile, with the increase of N, the length of the supports is getting longer and the regularity is getting better, which means the amplitude-frequency characteristic of Db Wavelets is getting

more ideal. The ideal amplitude-frequency characteristic of Db Wavelets is shown in Figure 3-3.

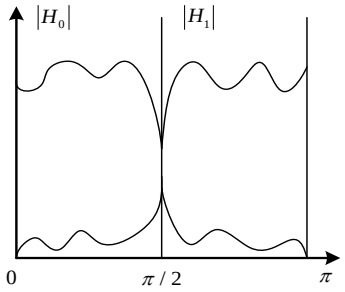

Figure 3-3 The ideal amplitude-frequency characteristic of Db Wavelet functions

It is obvious that Db Wavelets can be regarded as a combination of an ideal low-pass filter and an ideal high-pass filter. The more ideal the amplitude-frequency characteristic of Db Wavelets is, the better the Mallat Algorithm can be performed. As a general rule, to analyze the transient signal coming from power system, the Db Wavelets which has more vanishing moments, shorter length of the supports and better regularity are preferred. After adjusting the number and comparing the results, Db10 is chosen in this thesis.

The other parameter is the number of decomposition levels. It is preferable to use a higher decomposition level in order not to miss the features. However, as the decomposition level increases, the computational time becomes significantly larger. Therefore, it is crucial to select a suitable decomposition level that makes a good tradeoff between the number of candidate features and computing time. Reference [30] explains the calculation method about how to select the level of decomposition. It said that the minimum number of decomposition levels that is necessary for obtaining an approximation signal so that the

upper limit of its associated frequency band is under the fundamental frequency f is described by the following condition:

$$2^{-(n_{Ls}+1)} f_s < f \qquad \text{Equation 3-7}$$

Where n_{Ls} is the number of decomposition levels, f is the fundamental frequency and f_s is the sample frequency. f is 60 Hz in this microgrid and after changing the sample frequency and comparing the waveforms, f_s is set up as 400kHz in this thesis. Thus, based on these two values and the desire is that the main component in the first sub-band is fundamental frequency, after calculation, the level of decomposition is set up as 11 in this thesis.

Chapter 4 Simulation Results and Analysis

4.1 Description of Simulation Model

In this thesis, a simulation model of a DC microgrid with ground faults at different locations is built in MATLAB. The utility of grid is built in Simulink and the line to line voltage is set up as 208V. The model in Simulink is shown in Figure 4-1 and the relative parameters are shown in Figure 4-2.

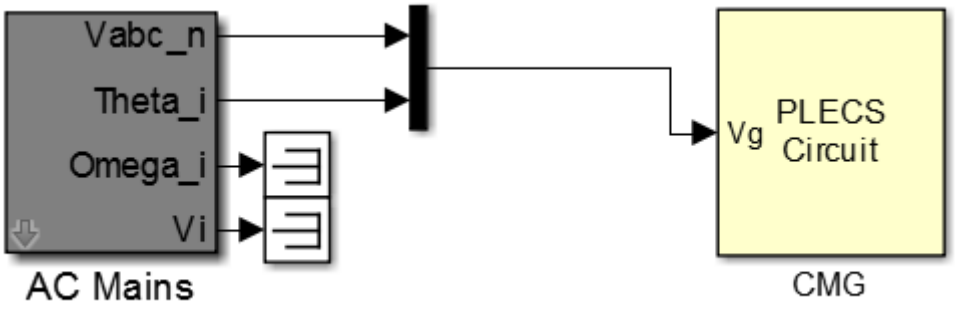

Figure 4-1 Simulation model in Simulink

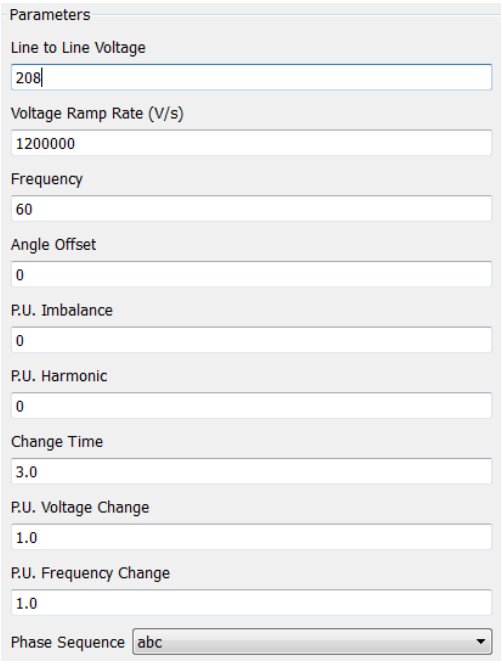

Figure 4-2 Parameters of the utility of grid

PLECS Blockset is embedded in MATLAB/Simulink as a toolbox, which is used to build the whole DC microgrid with ground faults. The model of DC microgrid is shown in Figure 4-3 and three critical simulation parameters in this model are shown in Table 4-1 Critical simulation parameters.

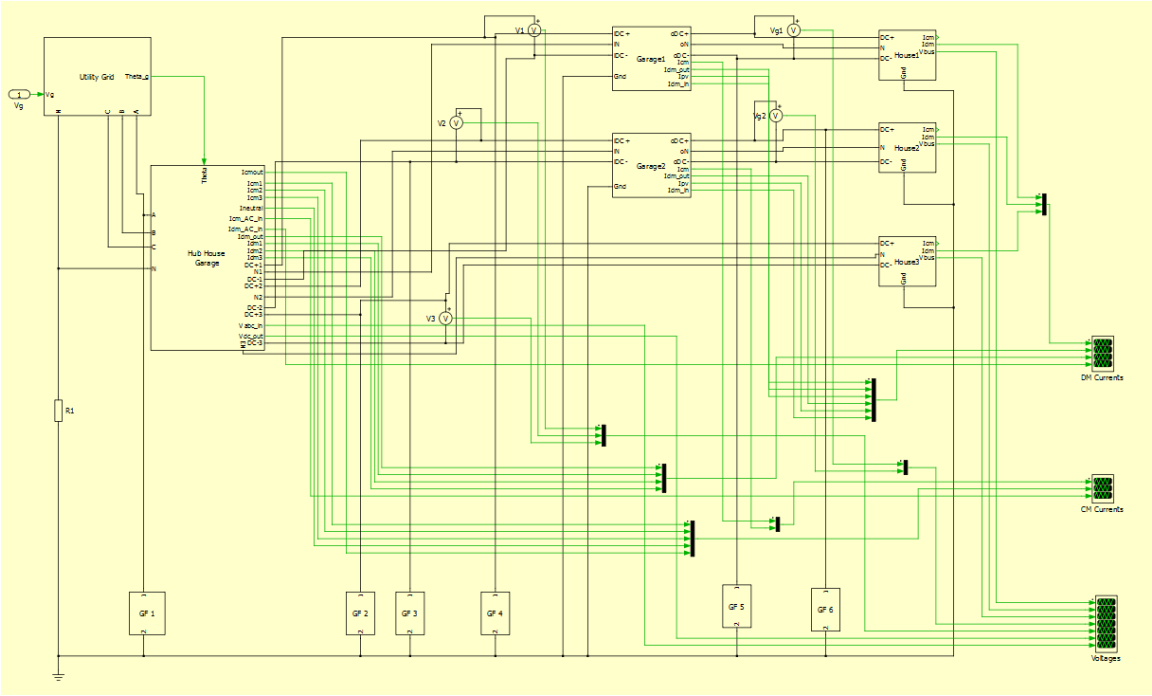

Figure 4-3 The simulation model of DC microgrid with ground faults

Table 4-1 Critical simulation parameters

Fault Application Time	0.65s
Sample Frequency	400kHz
Switching Frequency	10kHz

4.2 Characterization of Ground Faults

4.2.1 Normal Situation

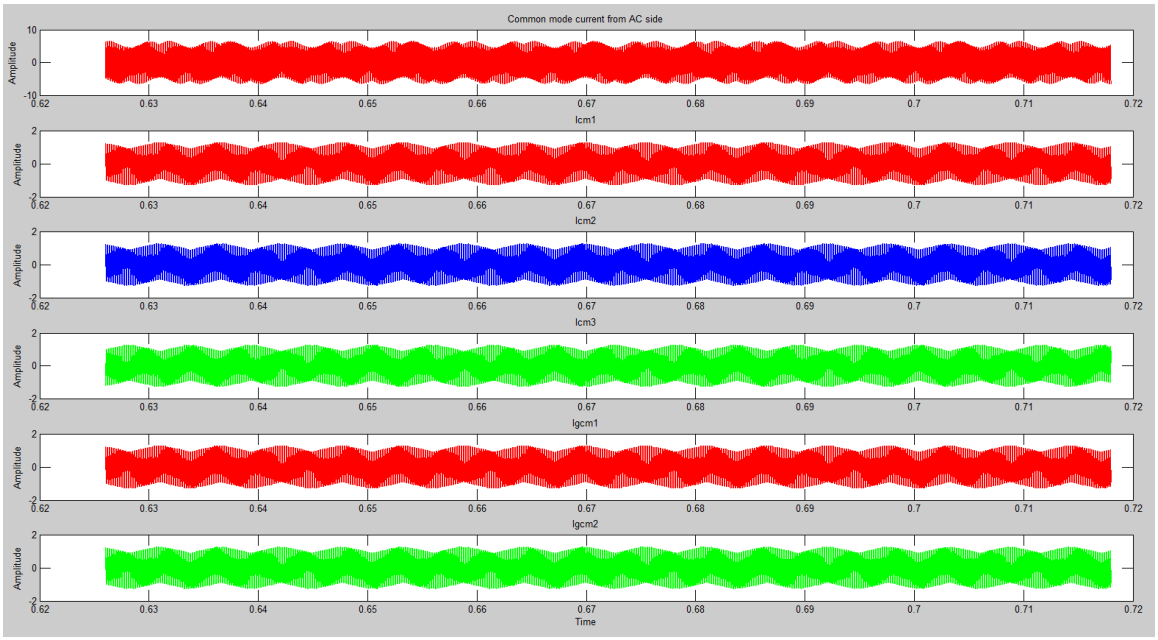

Figure 4-4 The CM currents from six sensors (Normal situation)

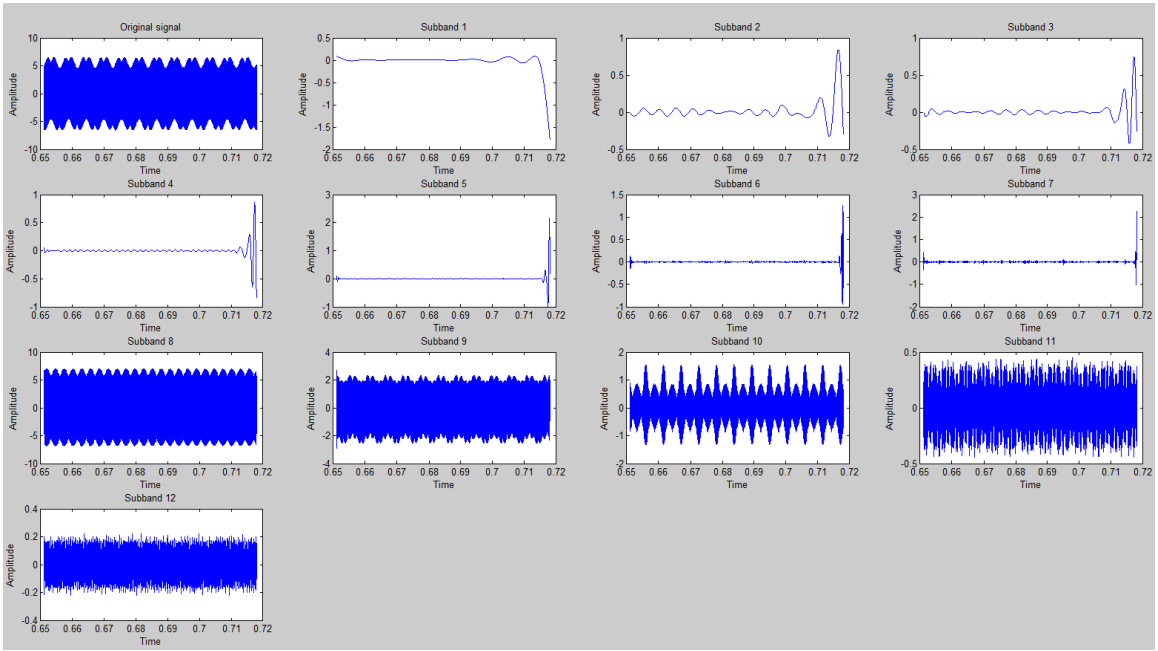

Figure 4-5 The decomposition results of CM currents coming from AC sensors (Normal situation)

Obviously, the original signals shown in Figure 4-4 are filled with high frequency components, which makes it difficult to capture the characteristics of these CM currents. So in order to find the unique characteristics, WT is applied and the decomposition results of the CM currents measured at AC side are shown in Figure 4-5. The process of achieving Figure 4-5 is: fault happens at 0.65s, and after 1ms delaying, the six sensors start to collect the data and the time range is from 0.651s to 0.72s, including four cycles. Then the original signals are decomposed and reconstructed into 12 sub signals by WT. The CM currents from other five sensors can also be decomposed and reconstructed through this process.

The first picture in Figure 4-5 is the original signal and the pictures left are the sub signals in corresponding sub-bands. From left to right, from the top down these sub-bands are named as Sb1 to Sb12. The frequency range of every sub-band is shown in Table 4-2 The frequency range of every sub-band.

Table 4-2 The frequency range of every sub-band

Sb1	**0Hz~97.65Hz**
Sb2	**97.65Hz~195.3Hz**
Sb3	**195.3Hz~390.6Hz**
Sb4	**390.6Hz~781.2Hz**
Sb5	**781.2Hz~1562.4Hz**
Sb6	**1562.4Hz~3124.8Hz**
Sb7	**3124.8Hz ~6249.6Hz**
Sb8	**6.25kHz~12.5kHz**
Sb9	**12.5kHz~25kHz**

Sb10	**25kHz~50kHz**
Sb11	**50kHz~100kHz**
Sb12	**100kHz~200kHz**

It is obvious that these 12 sub-bands can be divided into two categories based on the frequency range, which are low frequency sub-bands (Sb1 ~ Sb7) and high frequency sub-bands (Sb8 ~ Sb12). Considering about the accuracy, the signals and the results after 0.702s will be ignored.

In low frequency sub-bands, under normal situation, the amplitudes of waveforms are almost zero, which is exactly what is expected in power system. But if the single ground fault happened, the waveforms in low frequency sub-bands would change. And depending upon the location of the fault, the low frequency sub-bands will show different changes in waveforms and amplitudes, which we called characterizations. However, the waveforms in high frequency sub-bands do not change too much even during the fault. In other word, there is not much useful information in high frequency sub-bands. Given these two reasons, only first seven sub-bands (low frequency sub-bands) will be focused and analyzed in this thesis. Since the signal and the results after 0.702s have been ignored, there will be only three cycles analyzed, and the signal in the first cycle is a transient signal specifically. Thus, to capture the characterizations more precisely, every sub signal will be divided into two parts to be analyzed, which are transient part and stable part.

4.2.2 Single Phase-to-ground Fault

The single phase-to-ground fault is a ground fault that happens in AC system and it is called GF1 in this thesis. GF1 is at phase A and the flowing path of transient currents in the whole view is shown in Figure 4-6 The whole view of flowing path of currents (GF1).

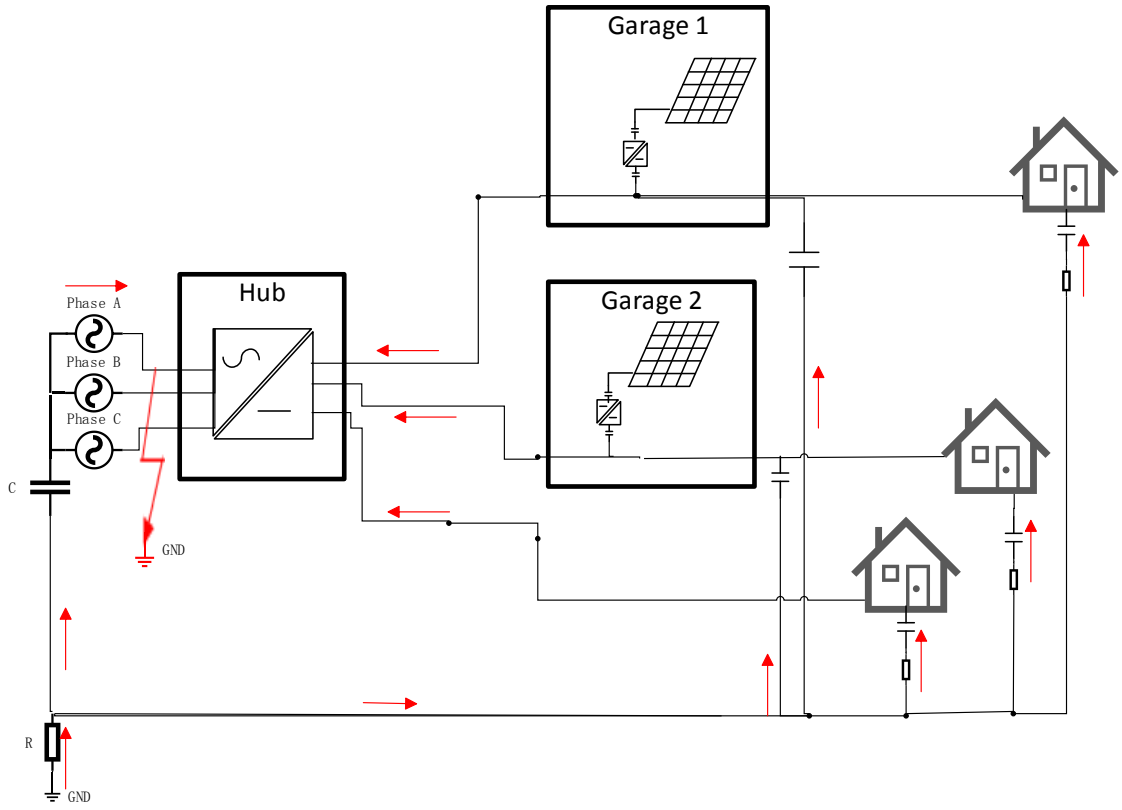

Figure 4-6 The whole view of flowing path of currents (GF1)

When the single ground fault happens in AC system, the grounding current will flow through all the stray capacitors in the DC system and then the currents in all branches will flow towards the AC side and feed the grounding current. Because of the unhealthy three phase voltages, ideal DM voltage of DC bus cannot be achieved, which results in the special waveforms that is shown in Figure 4-7. And these special waveforms are exactly the characterizations of GF1.

Figure 4-8 and Figure 4-9 show the decomposition results of the CM currents from AC sensors and Icm1. Because the waveforms from five sensors in DC system are similar with that from the sensor in AC system, the decomposition results of signals coming from DC system are also similar. By comparing Figure 4-8 and Figure 4-9, it is easy to find that the waveforms are almost the same, and only the amplitudes are different. The amplitude in DC system is smaller than that in AC system.

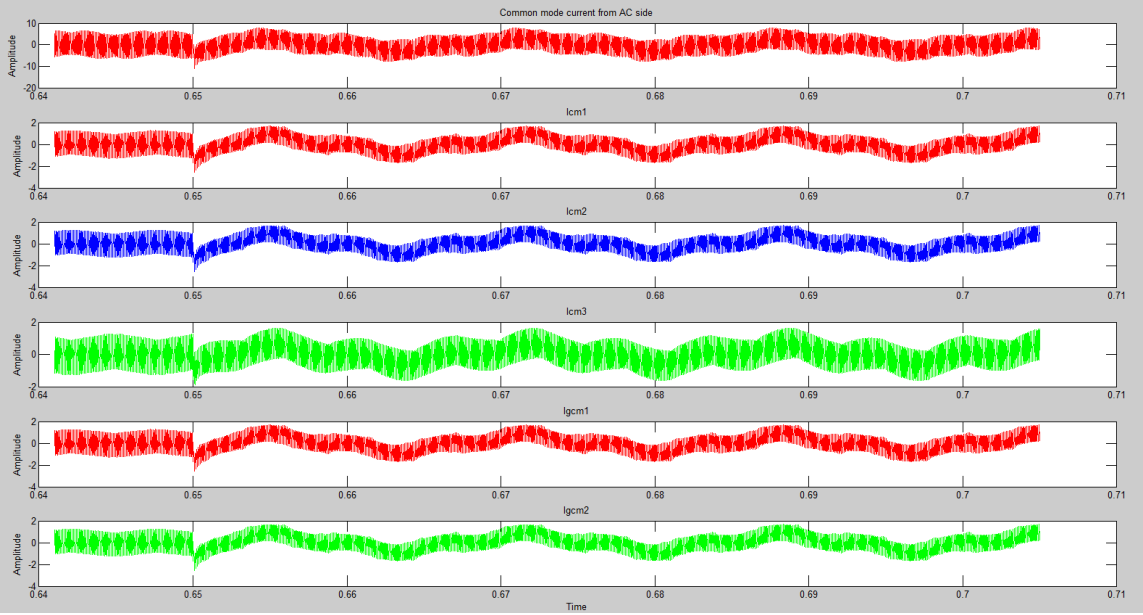

Figure 4-7 The CM currents from six sensors (GF1)

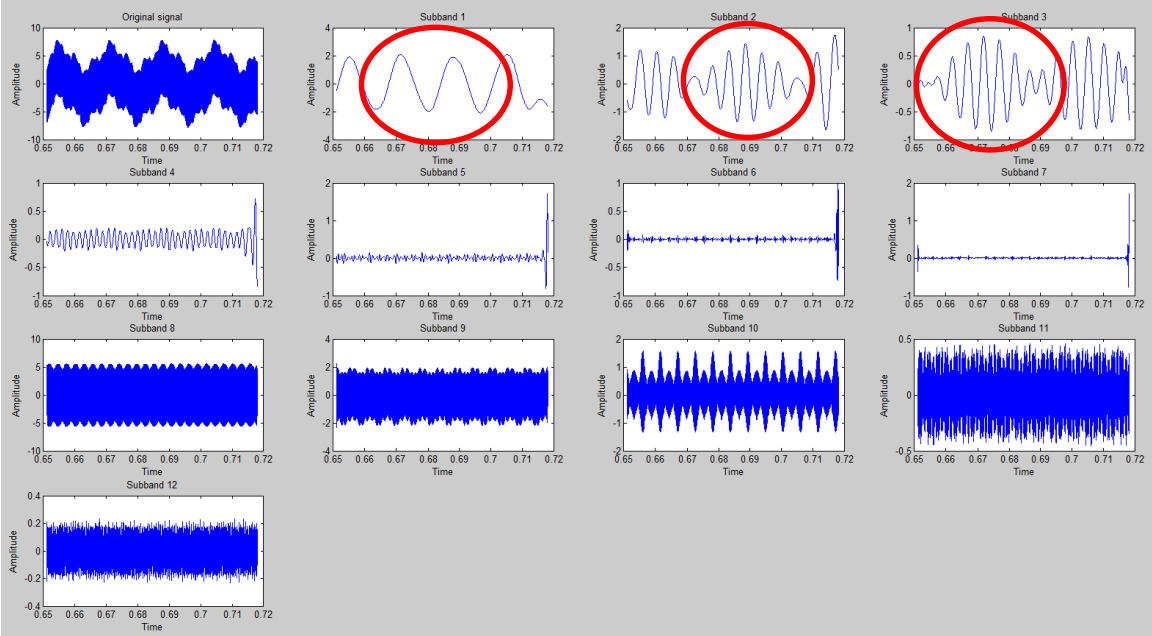

Figure 4-8 The decomposition results of CM currents from AC sensors (GF1)

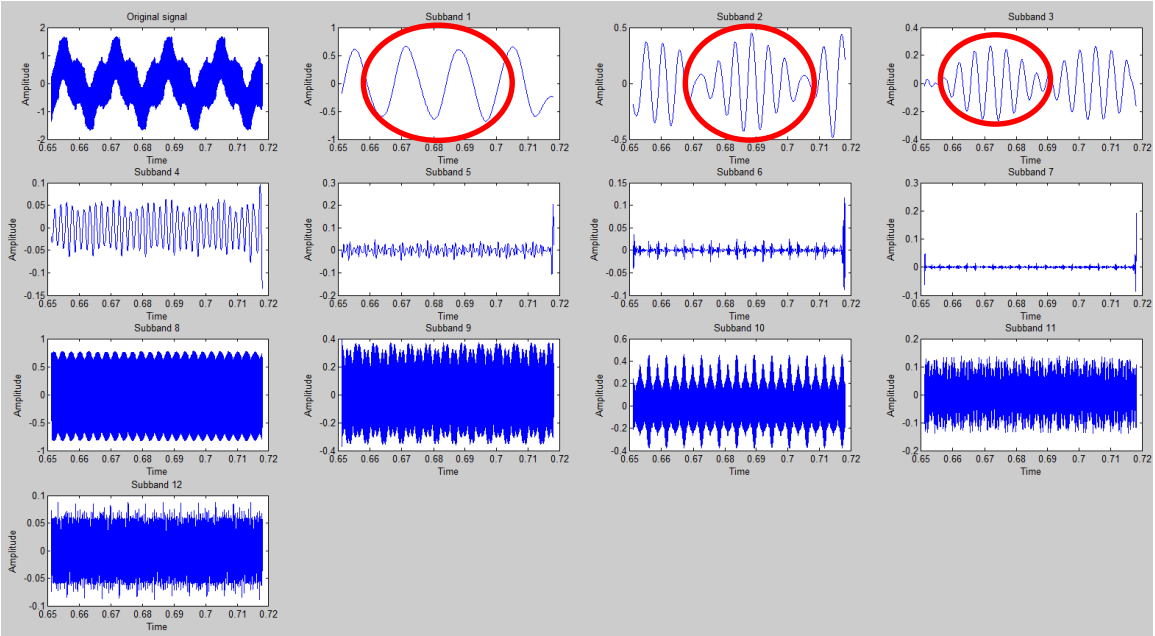

Figure 4-9 The decomposition results of Icm1 (GF1)

In conclusion, the biggest characterization of AC fault is the waveform. And basically, the currents from AC sensors only reflects the CM currents at the AC side and since the fault occurring in DC system does not affect the AC system much, the signal coming from AC sensors is not very helpful when it comes to locate the fault occurring in DC system.

4.2.3 Single Pole-to-ground Fault

Depends on the location, the single pole-to-ground faults can be divided into three categories, which are fault occurring near Hub, near Garage and in House. LV cables are used in Hub, Garages and Houses and if the fault happened between the cables used in Hub and the cables used in Garage, this kind of fault would be called the fault occurring near Hub. And if the fault happened after the cable used in House, this kind of fault would be called the fault occurring in House. Although there are PV panels at Feeder 1 and Feeder 2, since the simulation results show that they do not make any contributions in feeding ground fault, the problem can be simplified.

This section will cover the analysis of the three categories mentioned above.

4.2.2.1 Fault Occurring Near Hub

The first category to be discussed is the single pole-to-ground fault that occurs near Hub. There are three cases in this category. GF2 is a single pole-to-ground fault that occurs at Feeder 3 where there is no PV panel. GF3 and GF4 are single pole-to-ground faults that occurs at Feeder 2 and Feeder 1 where there are PV panels. The flowing paths of currents in the CM current equivalent circuit are shown from Figure 4-10 to Figure 4-12 The flowing paths of currents in CM current equivalent circuit (GF4).

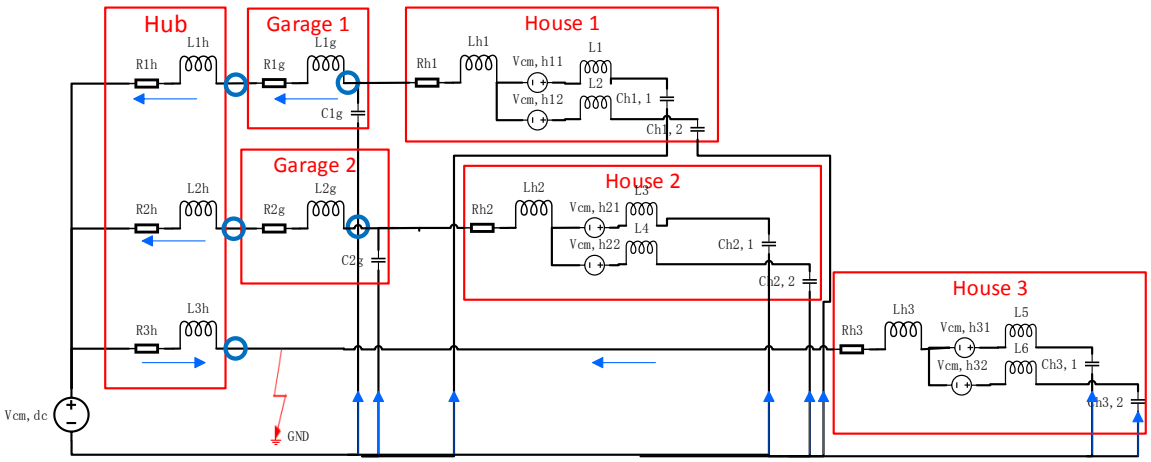

Figure 4-10 The flowing paths of currents in CM current equivalent circuit (GF2)

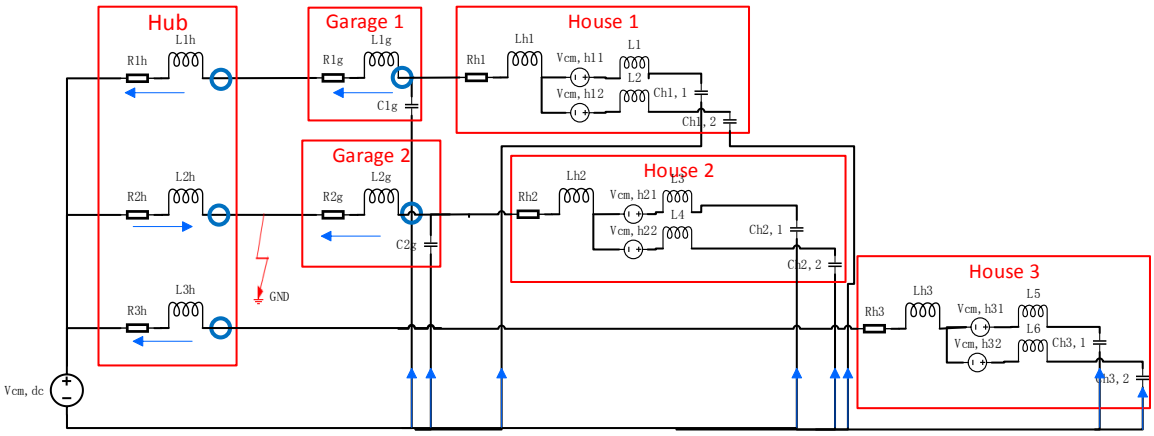

Figure 4-11 The flowing paths of currents in CM current equivalent circuit (GF3)

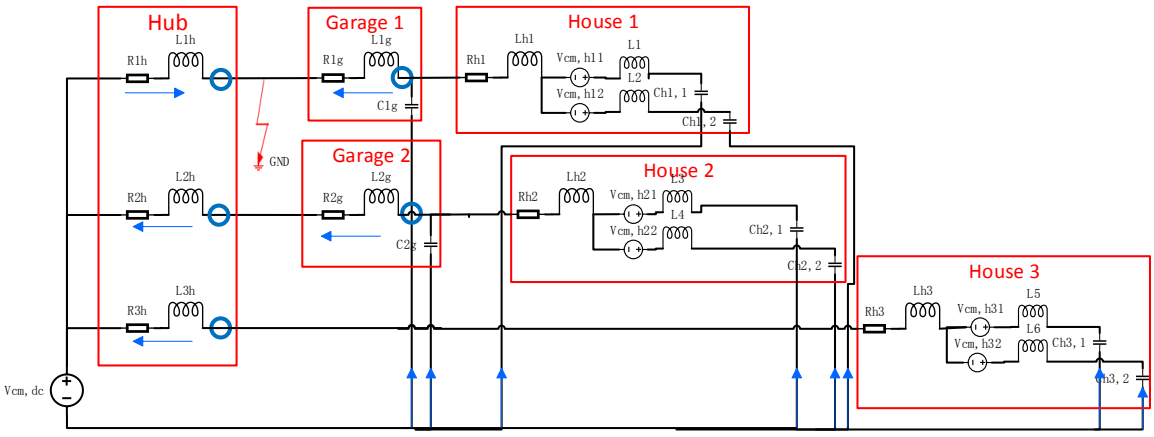

Figure 4-12 The flowing paths of currents in CM current equivalent circuit (GF4)

In these cases, the transient currents flowing through healthy feeders flow towards the AC/DC converter and try to feed the grounding current. And still, there are transient currents flowing through all the stray capacitors.

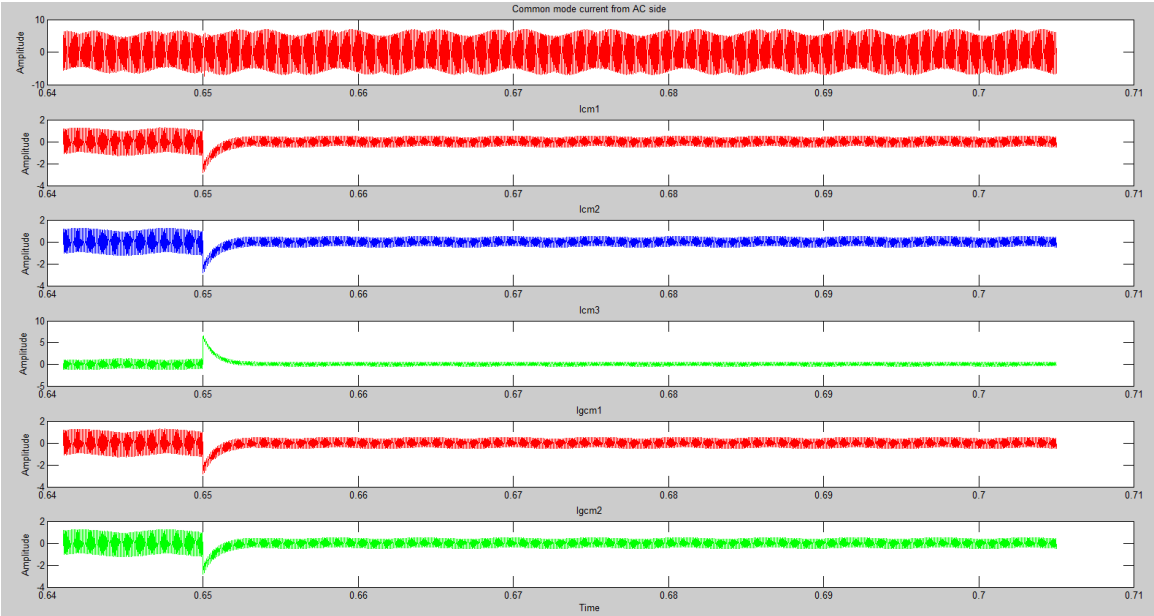

Figure 4-13 The CM currents from six sensors (GF2)

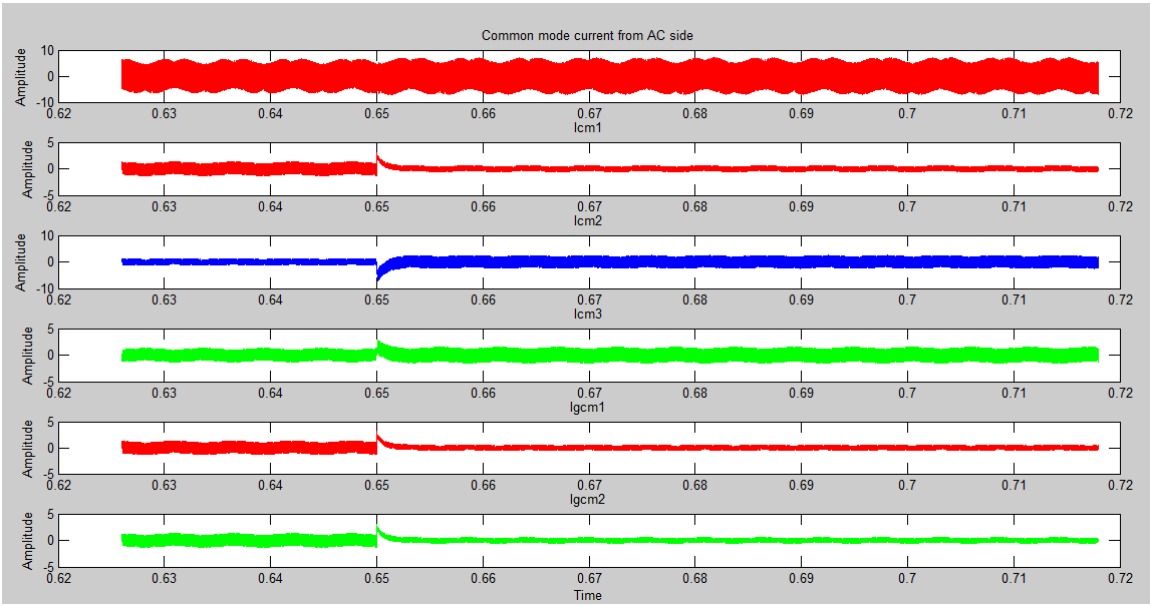

Figure 4-14 The CM currents from six sensors (GF3)

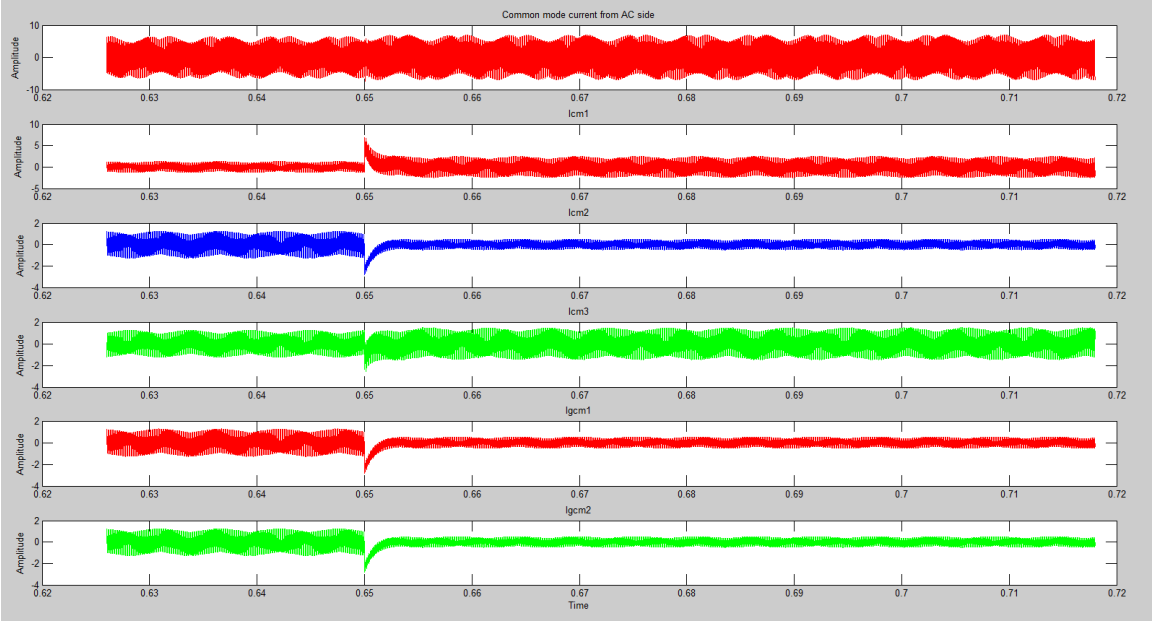

Figure 4-15 The CM currents from six sensors (GF4)

Figure 4-13, Figure 4-14 and Figure 4-15 show the CM currents from six sensors of these three cases. It is obvious that all of the currents measured in DC systems have a shift and return to stable status quite quickly. In contrast, the CM current measured in AC system does not change much, which is already explained in last section. Thus, the signal from AC sensors will not be used to locate the fault occurring in DC system.

Let us focused on the analysis of GF2. From Figure 4-16 to Figure 4-18, the decomposition results of Icm1, Icm2 and Icm3 are shown. Compared to normal situation, it is easy to find that there are some variations happening in low frequency sub-bands, especially in the first three sub-bands. In previous figures, the stable parts of the sub signals are almost zero, while in these cases, the sub signals have clear fluctuations even if the values are small. Table 4-3 shows the peak values in transient part and stable part of the first three sub-bands of Icm1, Icm2 and Icm3 respectively. It is obvious to be seen that the maximum values among all the peak values are coming from Feeder 3, which is the unhealthy feeder.

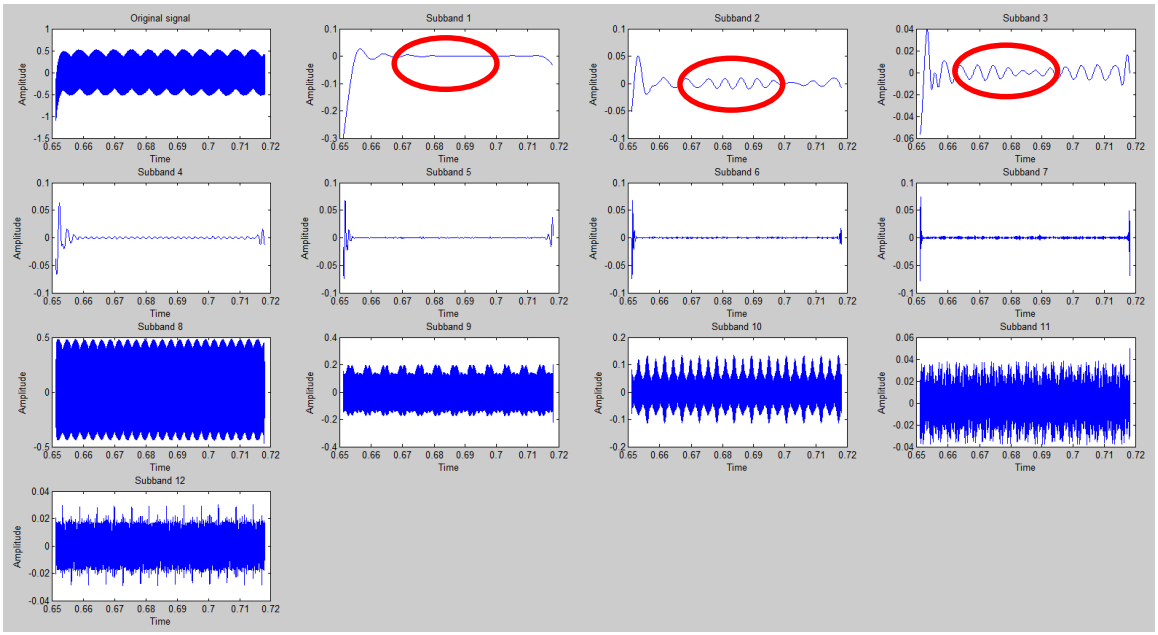

Figure 4-16 The decomposition results of Icm1 (GF2)

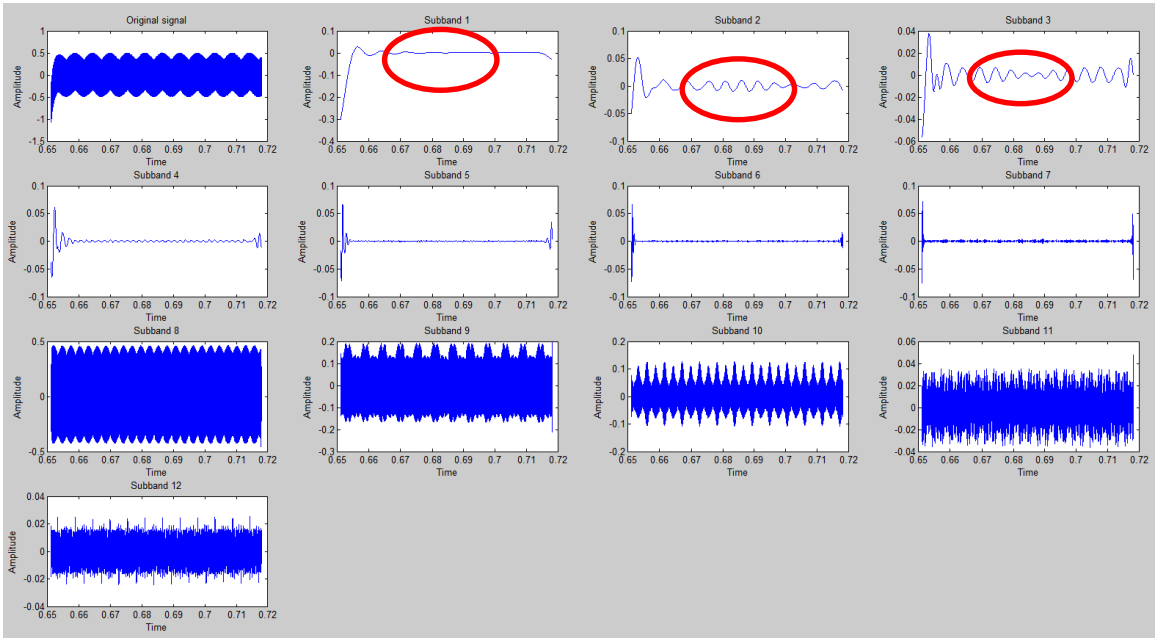

Figure 4-17 The decomposition results of Icm2 (GF2)

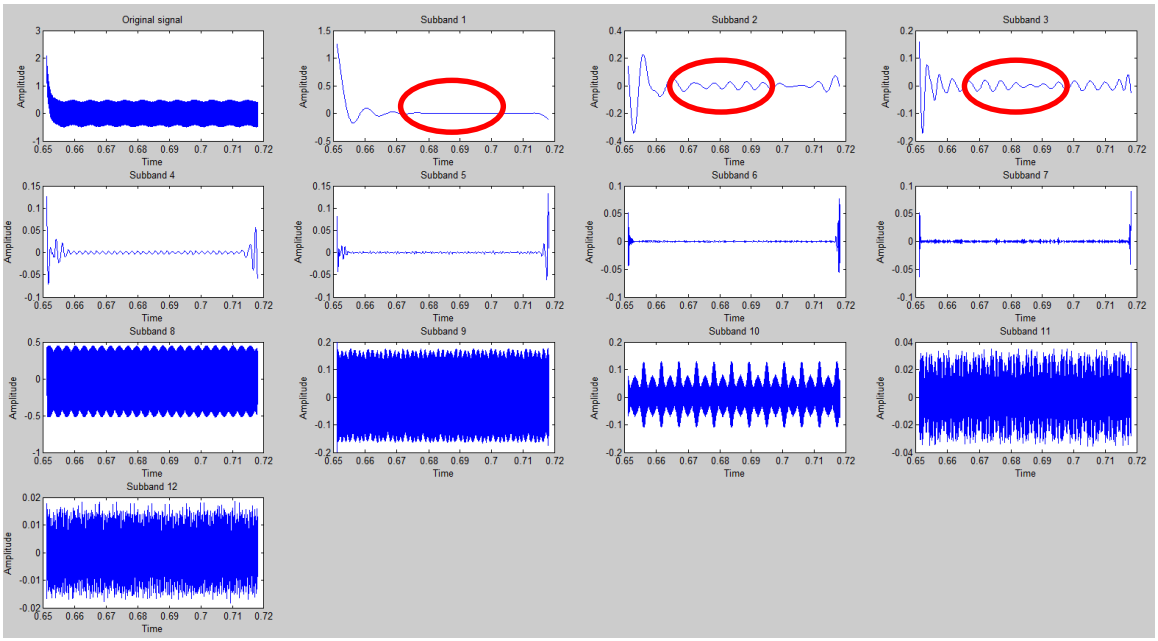

Figure 4-18 The decomposition results of Icm3 (GF2)

Table 4-3 The peak value of the first three sub-bands of Icm1 and Icm2 and Icm3 (GF2)

Icm1_1	0.0263	0.0047	**Icm2_1**	0.0271	0.0047	**Icm3_1**	1.2484	0.0291
Icm1_2	0.0501	0.0103	**Icm2_2**	0.0518	0.0103	**Icm3_2**	0.2281	0.0301
Icm1_3	0.0394	0.0068	**Icm2_3**	0.0378	0.0068	**Icm3_3**	0.1588	0.0210

Figure 4-19 and Figure 4-20 show the decomposition results of Igcm1 and Igcm2. Compared to normal situation, the results show the same variations with Figure 4-16 and Figure 4-17. Table 4-4 shows the peak values of the first three sub-bands of Igcm1 and Igcm2. And there is no obvious characteristics found in Table 4-4.

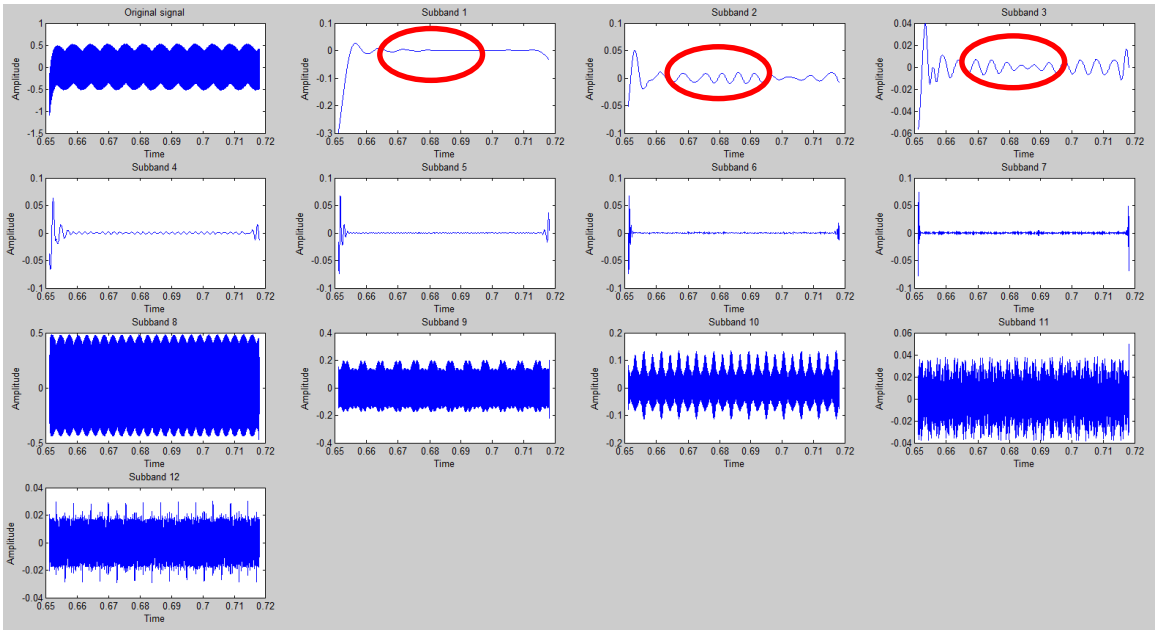

Figure 4-19 The decomposition results of Igcm1 (GF2)

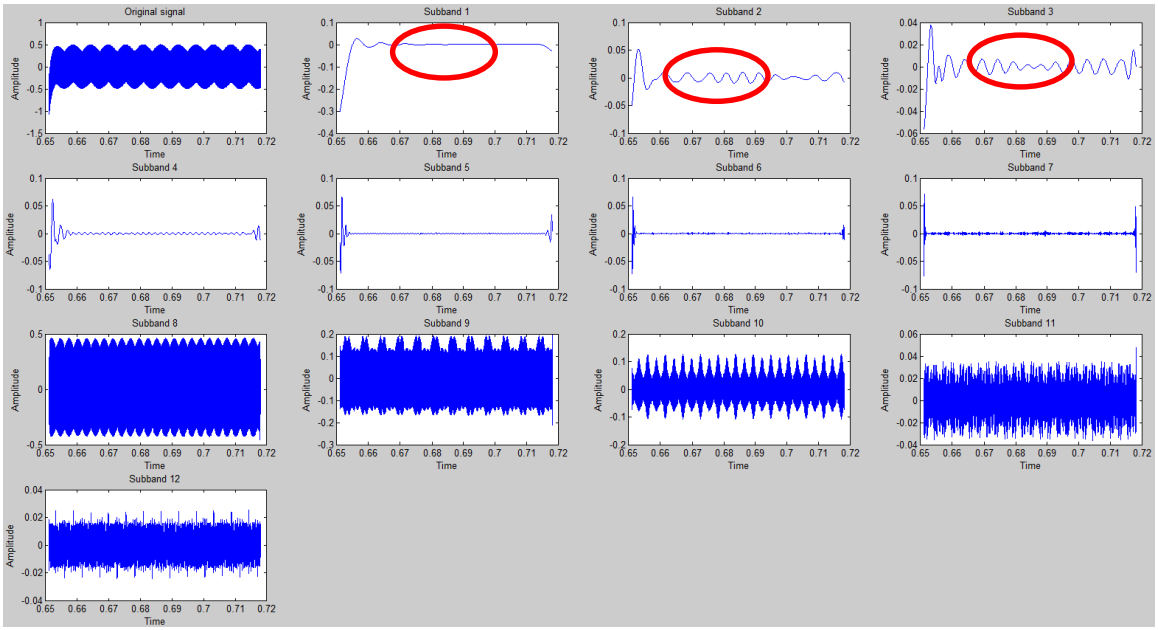

Figure 4-20 The decomposition results of Igcm2 (GF2)

Table 4-4 The peak value of first three sub-bands of Igcm1 and Igcm2 (GF2)

Igcm1_1	0.0263	0.0047	**Igcm2_1**	0.0271	0.0047
Igcm1_2	0.0501	0.0103	**Igcm2_2**	0.0518	0.0103
Igcm1_3	0.0394	0.0068	**Igcm2_3**	0.0378	0.0068

About other two cases, which are GF3 and GF4, they show similar waveforms and values so they are not discussed any more. This kind of waveforms and these values can be regarded as the characterizations of this kind of fault and Section 4.3 will present how to use these characterizations to locate these three single ground faults in detail.

4.2.2.2 Fault Occurring Near Garage

The second category to be discussed is the single pole-to-ground fault that occurs near Garages. Since there is no PV panel at Feeder 3, there are only two cases in this category. GF5 is a single pole-to-ground fault that occurs at Feeder 1 and GF6 is a single pole-to-ground faults that occurs at Feeder 2. The flowing paths of currents in the CM current equivalent circuit are shown in Figure 4-21 and Figure 4-22.

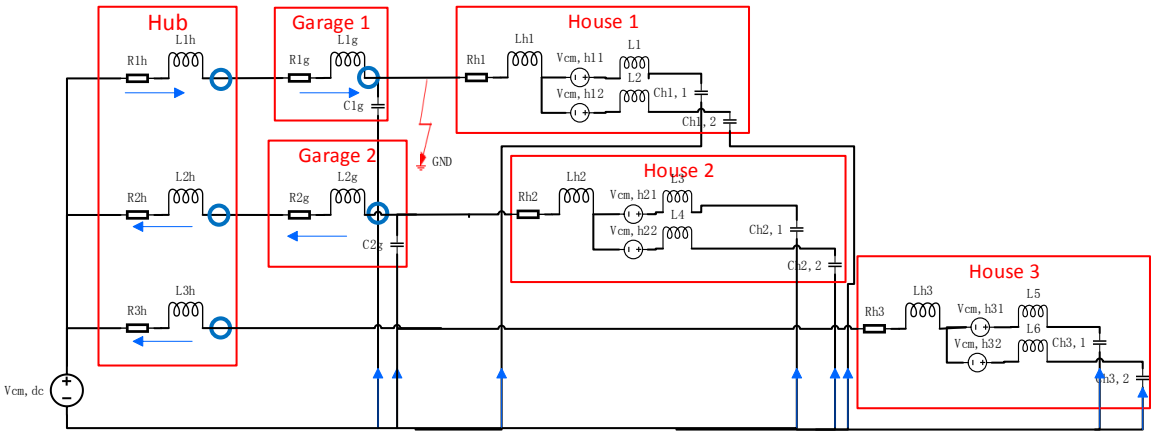

Figure 4-21 The flowing paths of currents in CM current equivalent circuit (GF5)

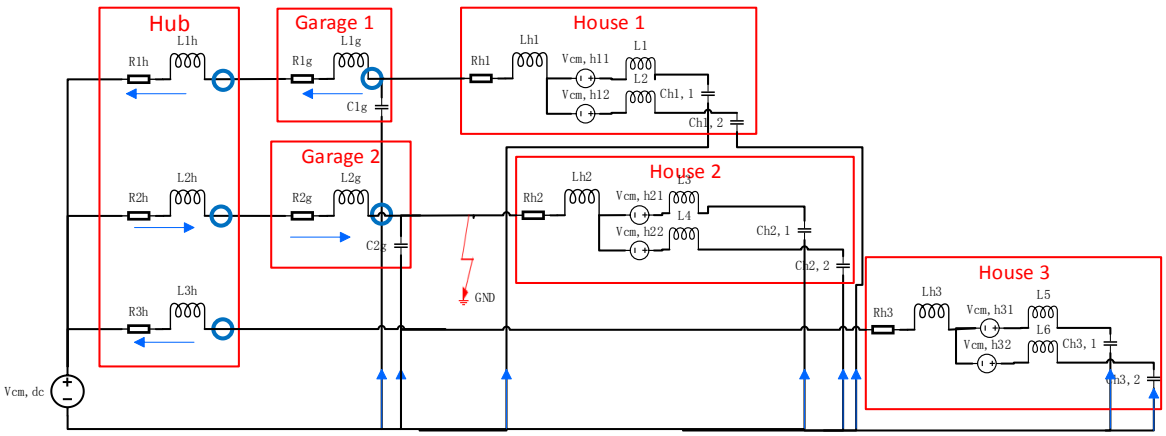

Figure 4-22 The flowing paths of currents in CM current equivalent circuit (GF6)

Figure 4-23 and Figure 4-24 show the CM currents from six sensors of these two cases. Also, in these two cases, all of the CM currents measured in DC systems have a shift and return to stable status quite quickly.

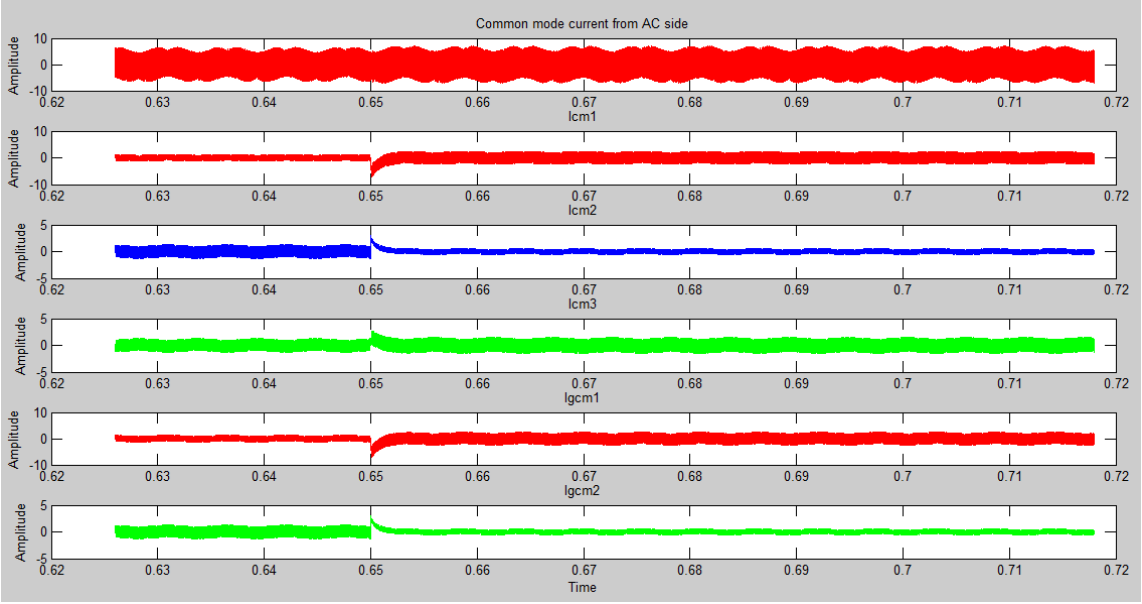

Figure 4-23 The CM currents from six sensors (GF5)

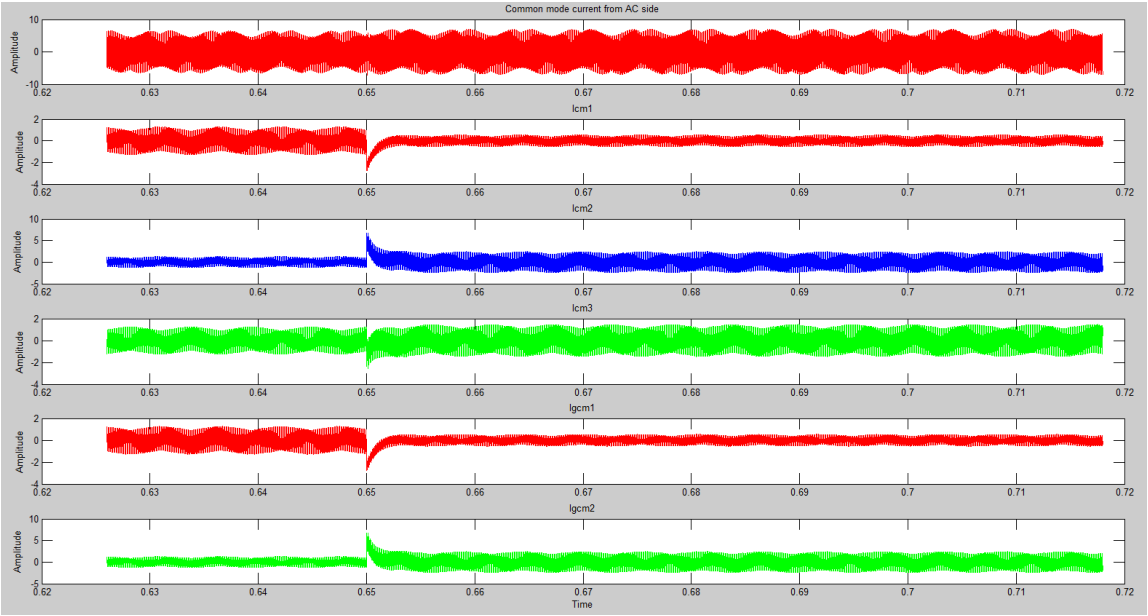

Figure 4-24 The CM currents from six sensors (GF6)

Let us focused on the analysis of GF6. From Figure 4-25 to Figure 4-27Figure 4-18, the decomposition results of Icm1, Icm2 and Icm3 are shown. Similar with GF2, there are also some variations happening in low frequency sub-bands, especially in first three sub-bands. Table 4-5 shows the peak values in transient part and stable part of first three sub-bands of Icm1, Icm2 and Icm3 respectively. In this case, the maximum values among all the peak values are still coming from the unhealthy feeder, which is Feeder 2.

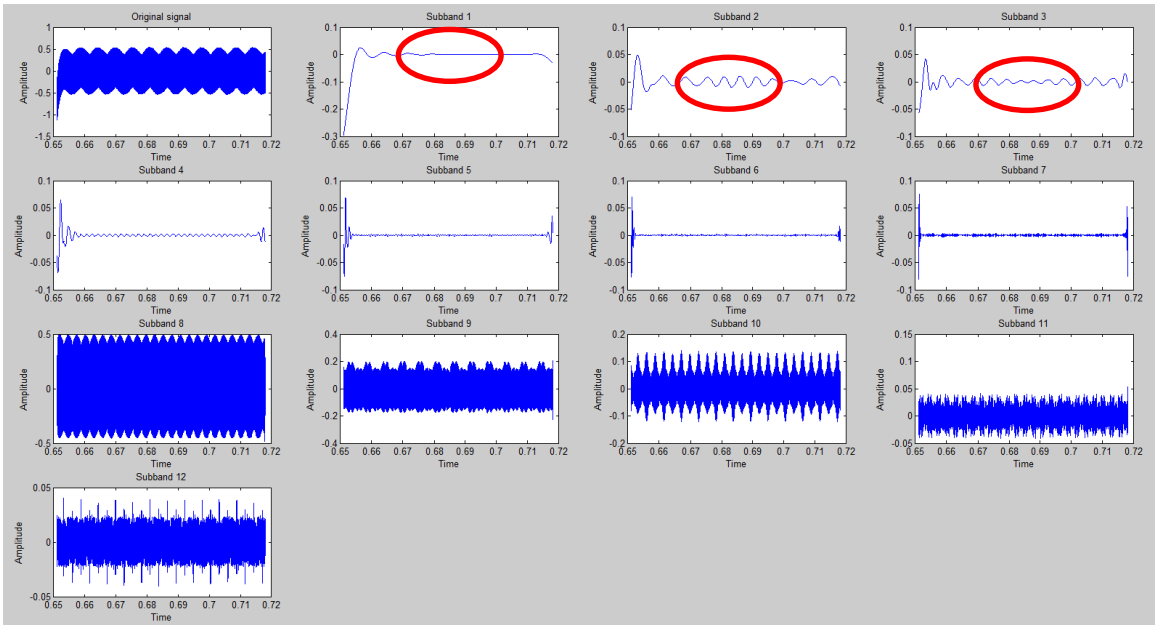

Figure 4-25 The decomposition results of Icm1 (GF6)

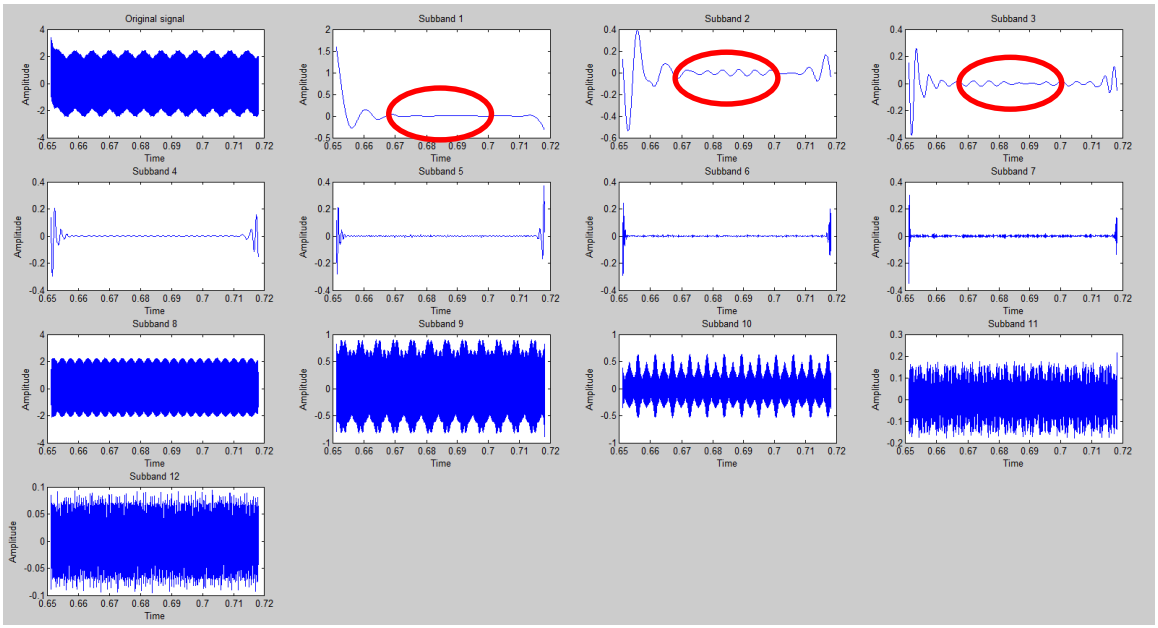

Figure 4-26 The decomposition results of Icm2 (GF6)

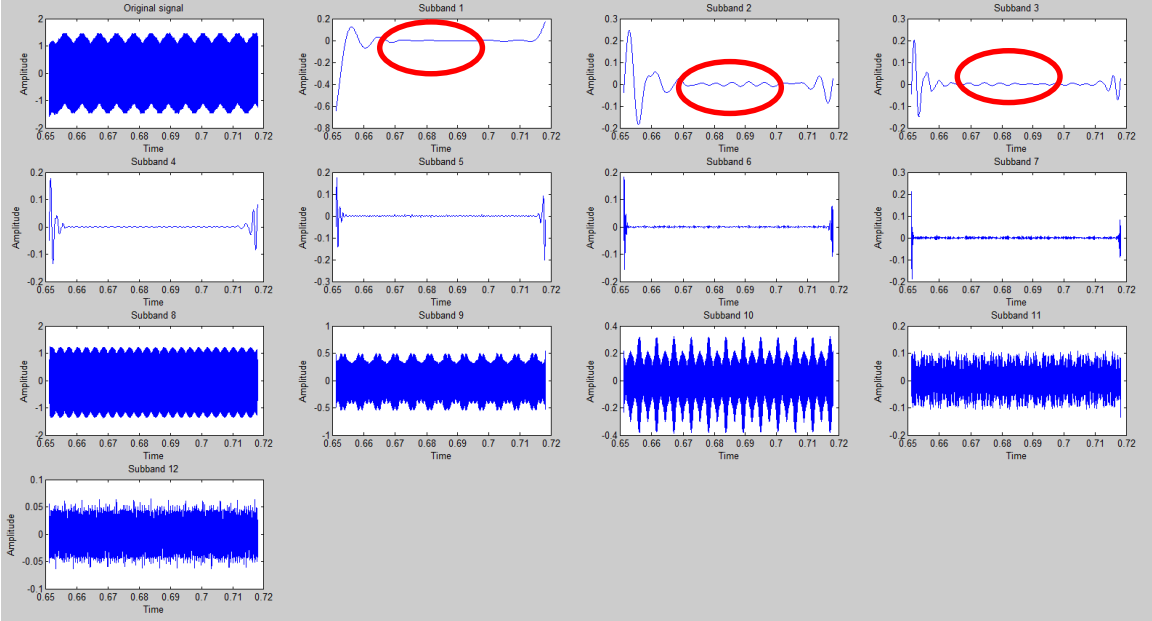

Figure 4-27 The decomposition results of Icm3 (GF6)

Table 4-5 The peak value of first three sub-bands of Icm1 and Icm2 and Icm3 (GF6)

Icm1_1	0.0250	0.0048	**Icm2_1**	1.5846	0.0430	**Icm3_1**	0.1243	0.0050
Icm1_2	0.0488	0.0106	**Icm2_2**	0.3911	0.0308	**Icm3_2**	0.2439	0.0237
Icm1_3	0.0418	0.0066	**Icm2_3**	0.2592	0.0192	**Icm3_3**	0.2014	0.0069

Figure 4-28 and Figure 4-29Figure 4-18 show the decomposition results of Igcm1 and Igcm2. Table 4-6 shows the peak values in transient part and stable part of first three sub-bands of Igcm1 and Igcm2. In Table 4-4, there is no big difference between the unhealthy feeder and healthy feeders. However, in this case, a characteristic can be found in Table 4-6 based on the peak values, which is the peak values at unhealthy feeder (Feeder 2) are much higher than those at healthy feeder (Feeder 1). This is exactly a big characteristic that can help to tell if the fault happens before the Garages or after the Garages.

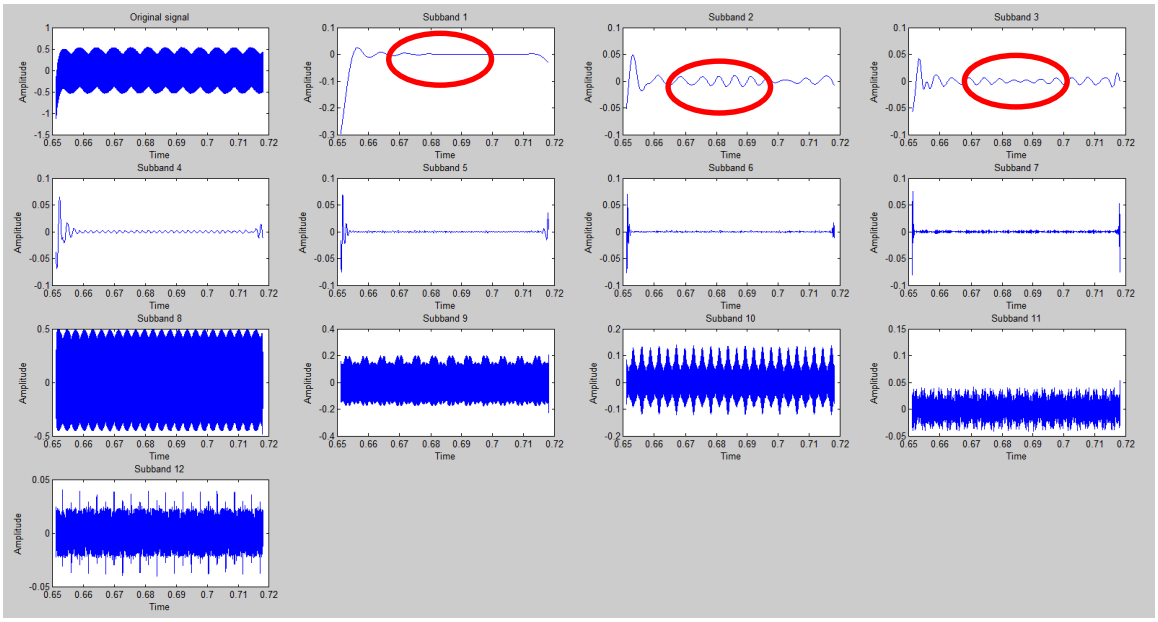

Figure 4-28 The decomposition results of Igcm1 (GF6)

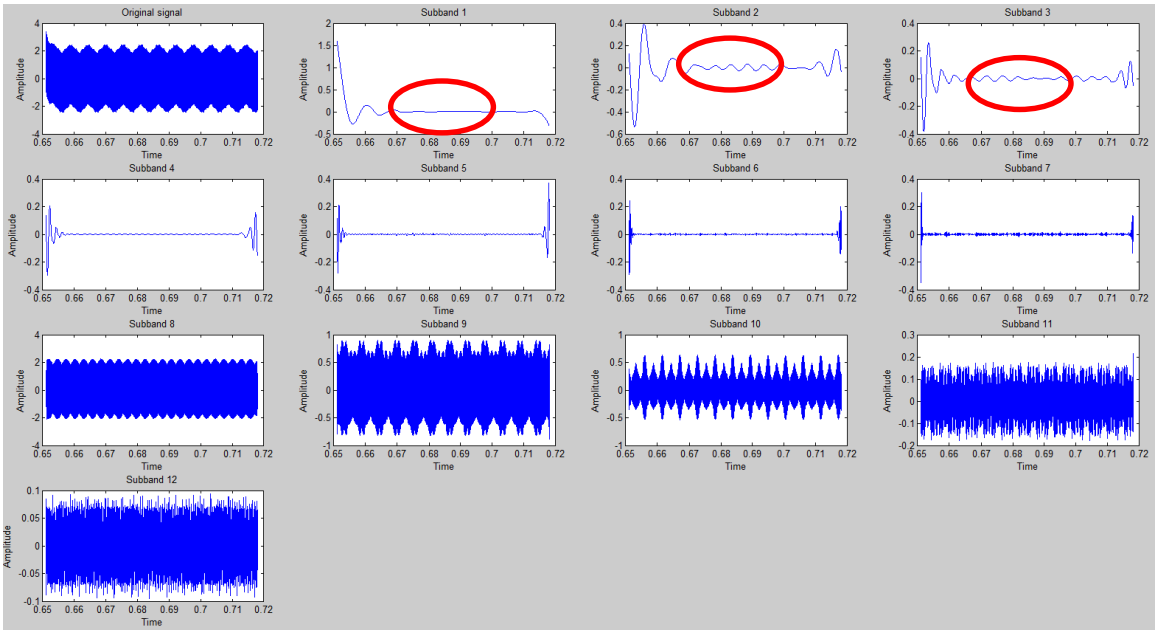

Figure 4-29 The decomposition results of Igcm2 (GF6)

Table 4-6 The peak value of first three sub-bands of Igcm1 and Igcm2 (GF6)

Igcm1_1	0.0250	0.0048	**Igcm2_1**	1.5846	0.0430
Igcm1_2	0.0488	0.0106	**Igcm2_2**	0.3911	0.0308
Igcm1_3	0.0418	0.0066	**Igcm2_3**	0.2592	0.0192

4.2.2.3 Fault Occurring in Houses

The third category to be discussed is the single pole-to-ground fault that occurs near the Houses. The fault happening in the House 1 is called GF71, and GF72 and GF73 are based on the same definition. The flowing paths of currents of GF71, GF72 and GF73 are shown from Figure 4-30 to Figure 4-32. And from Figure 4-33 to Figure 4-35, the CM currents from six sensors of these three cases are shown. Compared with the CM currents of previous two categories, given the two DC/DC converters in the house, the waveforms of CM currents are quite different and supposed to have more transient and high frequency components, which will be noticed in the decomposition results.

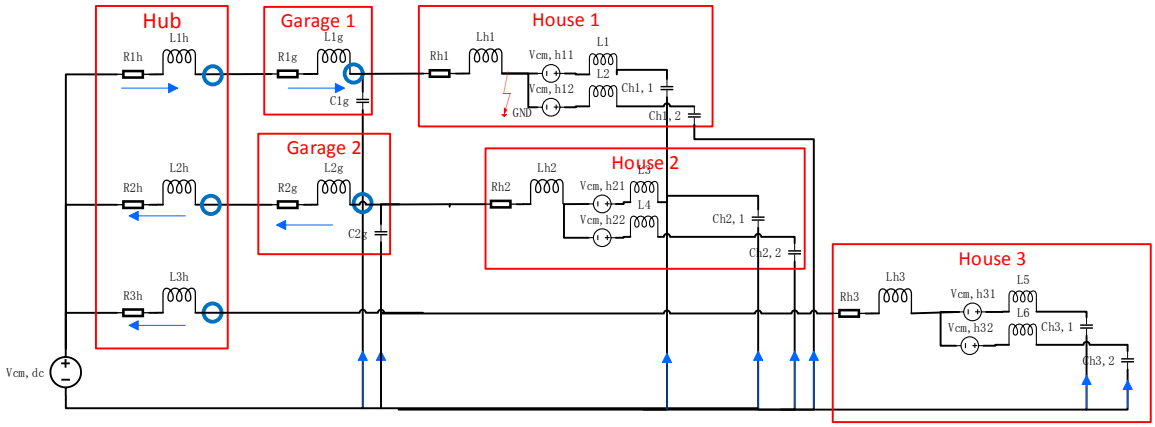

Figure 4-30 The flowing path of currents in CM current equivalent circuit (GF71)

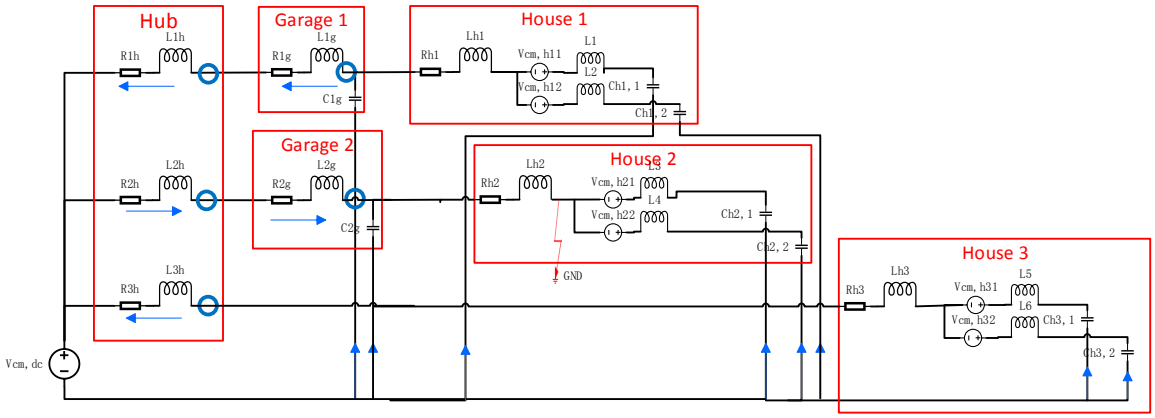

Figure 4-31 The flowing path of currents in CM current equivalent circuit (GF72)

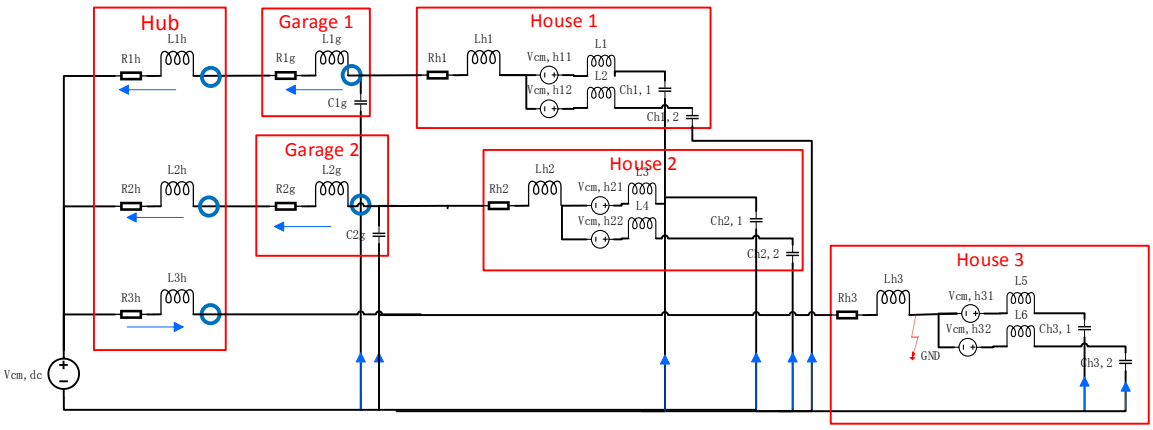

Figure 4-32 The flowing path of currents in CM current equivalent circuit (GF73)

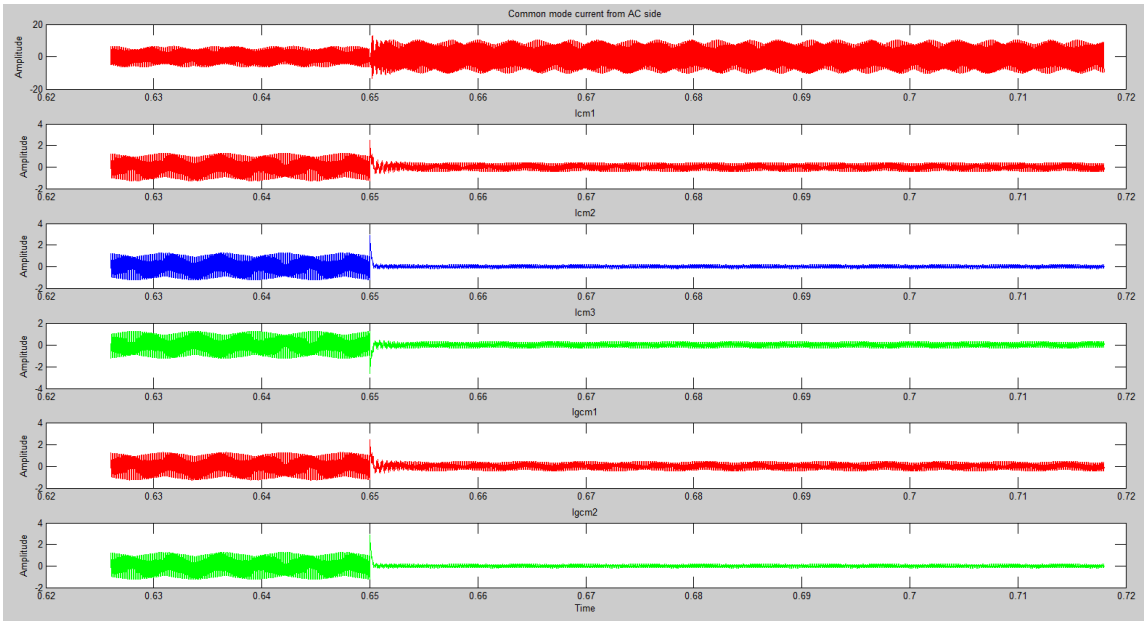

Figure 4-33 The CM currents from six sensors (GF71)

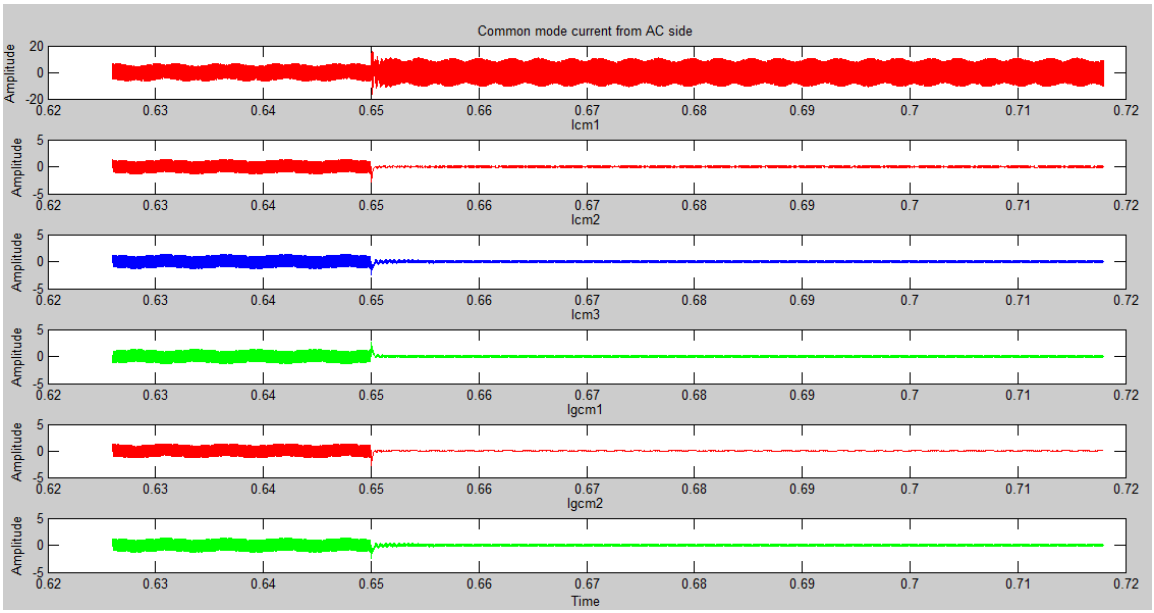

Figure 4-34 The CM currents from six sensors (GF72)

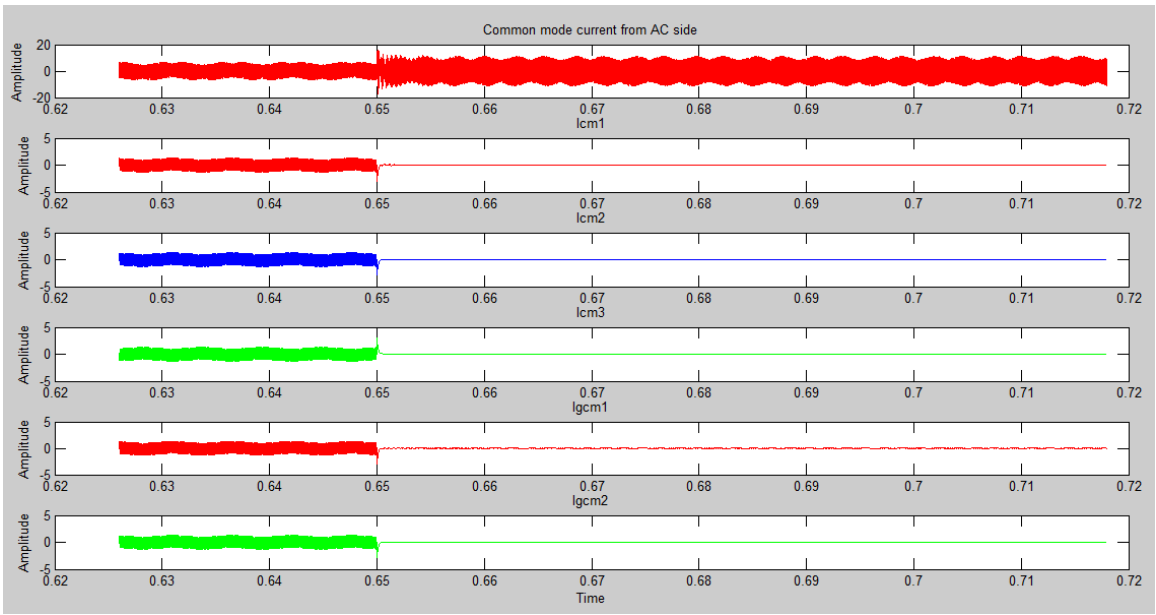

Figure 4-35 The CM currents from six sensors (GF73)

Same with what is done in previous two categories, let us focus on analyzing GF71 in this category. The decomposition results of Icm1, Icm2 and Icm3 are shown from Figure 4-36 to Figure 4-38 and there are two remarkable things should be noticed. The first one is that the variations in first three sub-bands are much smaller and the status parts are almost zero compared with previous results. And the other one is about the interesting variations in the

6^{th} and 7^{th} sub-bands. After zooming in the transient part of the 6^{th} sub-band of Icm1, the comparison results of three categories are shown in Figure 4-39. From left to right, the sub signals in the 6^{th} sub-band are coming from GF1, GF4 and GF71. It is obvious to find that GF71 has longer transient and damping process because of the DC/DC converters. And it is no doubt that this visible characteristic can be used to distinguish the ground fault occurring in Houses from other kinds of ground fault.

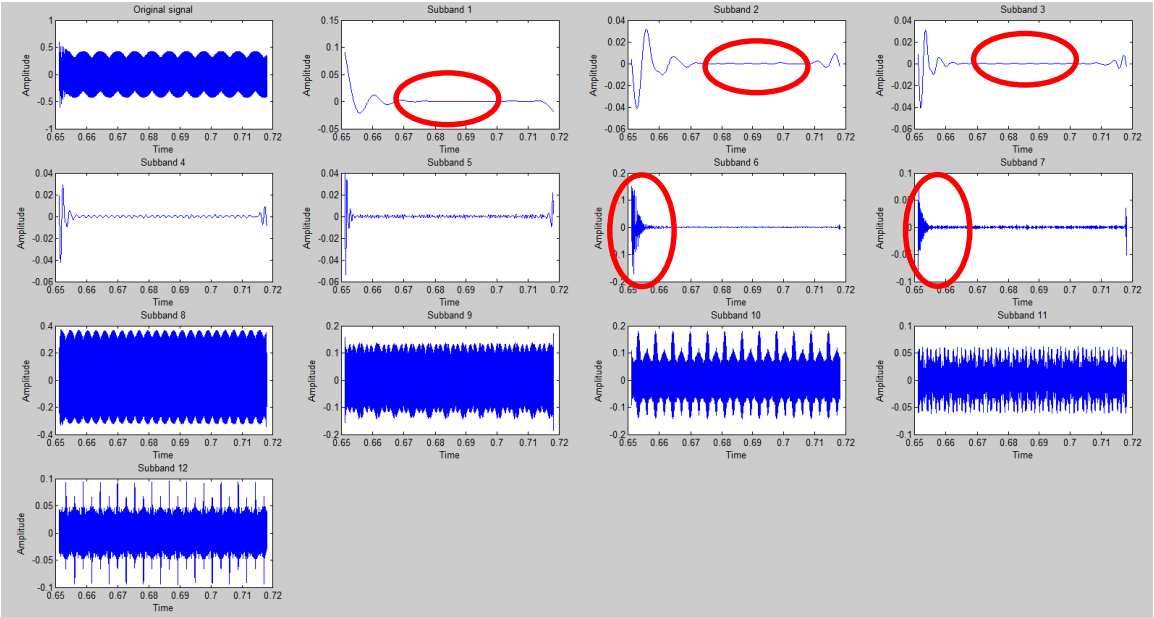

Figure 4-36 The decomposition results of Icm1 (GF71)

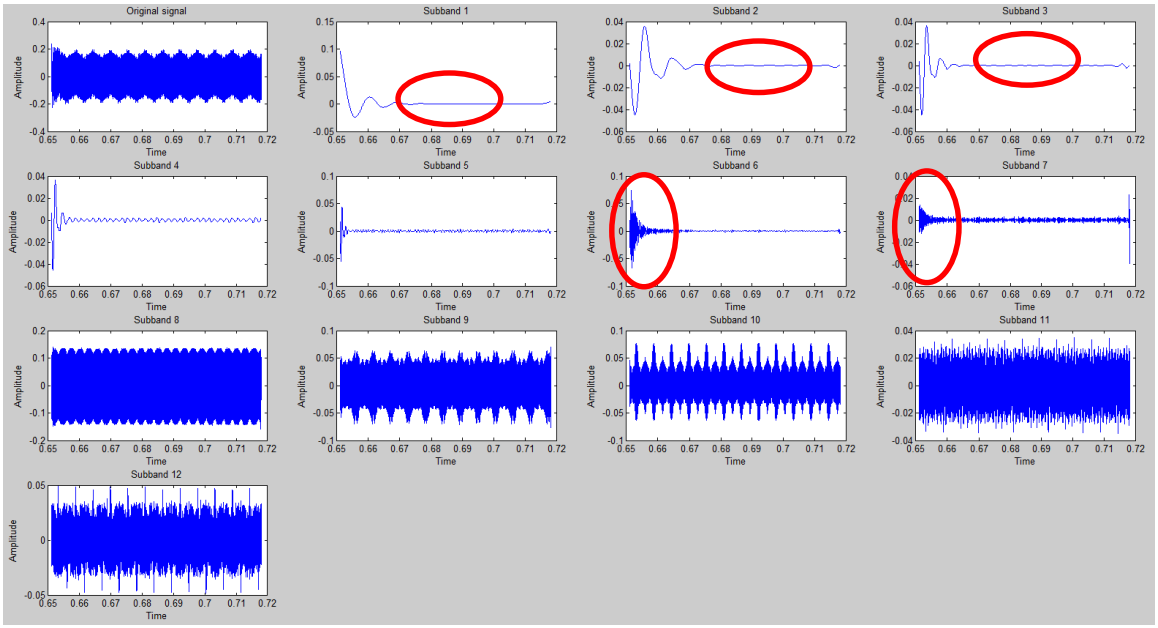

Figure 4-37 The decomposition results of Icm2 (GF71)

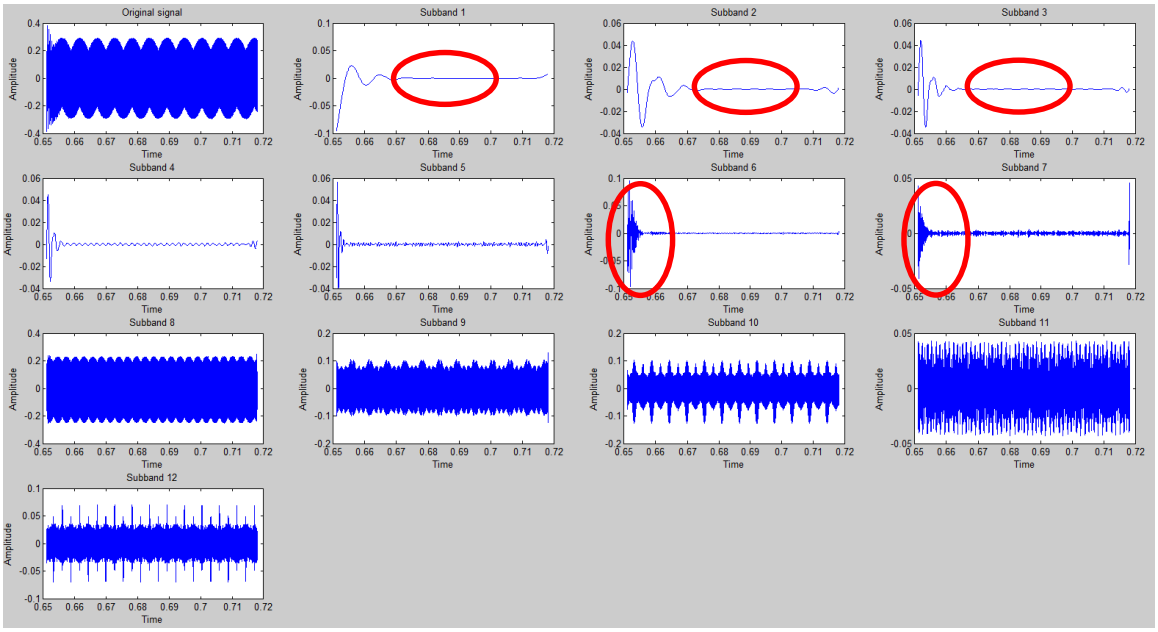

Figure 4-38 The decomposition results of Icm3 (GF71)

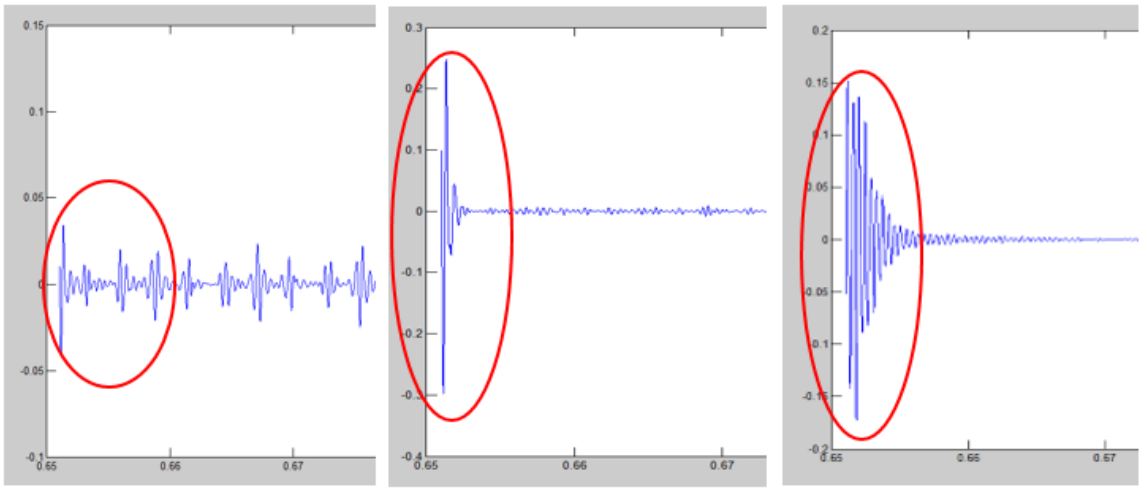

Figure 4-39 The comparison result of the 6th sub-band of Icm1

Table 4-7 shows the peak value of first three sub-bands of Icm1 and Icm2 and Icm3 (GF71). Same with previous analysis, the maximum value would come from the unhealthy feeder.

Table 4-7 The peak value of first three sub-bands of Icm1 and Icm2 and Icm3 (GF71)

Icm1_1	0.0964	0.0033	**Icm2_1**	0.0904	0.0033	**Icm3_1**	0.0229	0.0009
Icm1_2	0.0357	0.0035	**Icm2_2**	0.0317	0.0008	**Icm3_2**	0.0338	0.0011
Icm1_3	0.0362	0.0003	**Icm2_3**	0.0309	0.0001	**Icm3_3**	0.0342	0.0001

Figure 4-40 and Figure 4-41 show the decomposition results of Igcm1 and Igcm2. Those low frequency sub-bands show similar characteristics with what have been found in Figure 4-36, Figure 4-37 and Figure 4-38. And Table 4-8 shows that the peak values at unhealthy feeder (Feeder 1) are much higher than those at healthy feeder (Feeder 2), which is similar with GF6. And also, the maximum value happens at Feeder 1 where House 1 (location of the single ground fault) is.

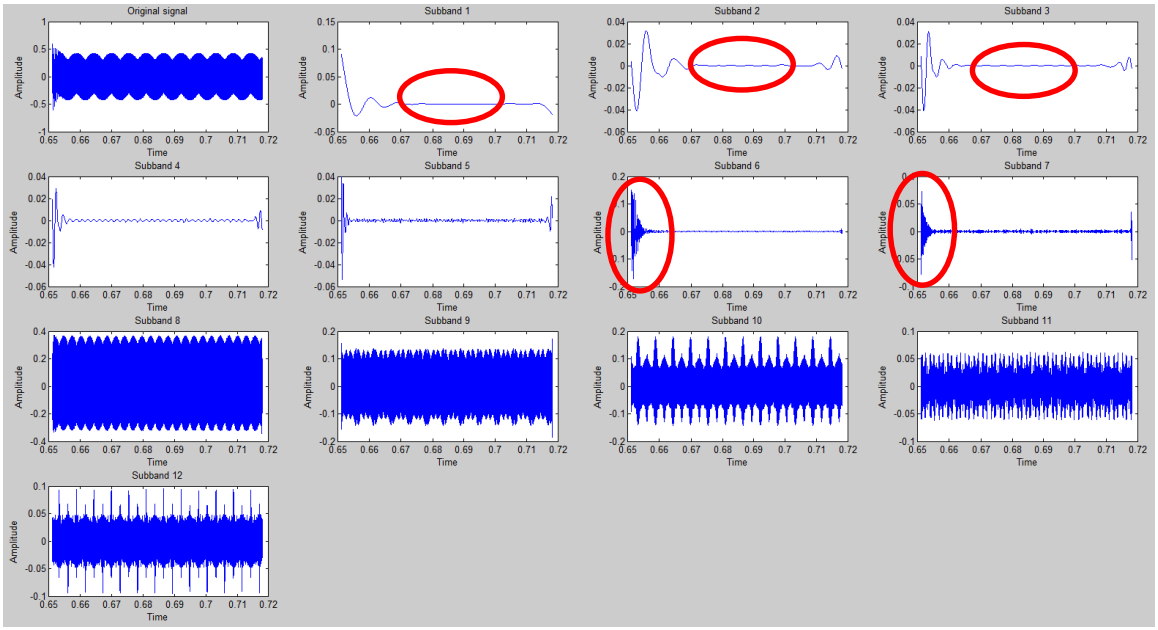

Figure 4-40 The decomposition results of Igcm1 (GF71)

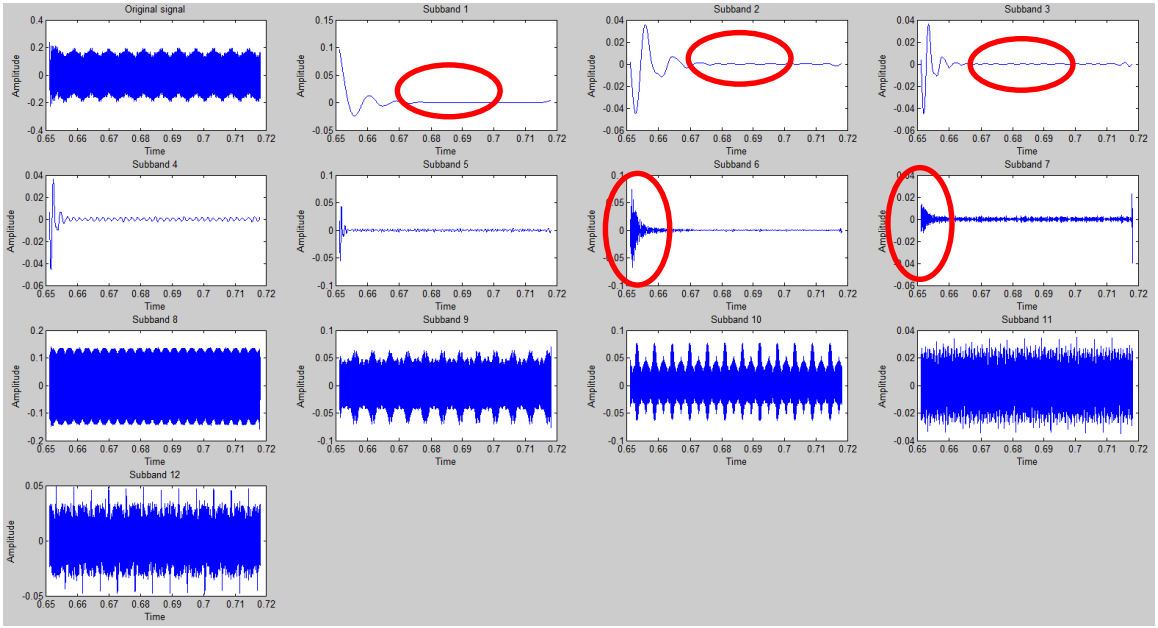

Figure 4-41 The decomposition results of Igcm2 (GF71)

Table 4-8 The peak value of first three sub-bands of Igcm1 and Igcm2(GF71)

Igcm1_1	0.0964	0.0033	**Igcm2_1**	0.0904	0.0033
Igcm1_2	0.0357	0.0035	**Igcm2_2**	0.0317	0.0008
Igcm1_3	0.0362	0.0003	**Igcm2_3**	0.0309	0.0001

4.2.4 Summary

From Section 4.2.1 to Section 4.2.3, normal situation and all kinds of single ground fault are analyzed and some basic characterizations which can be used to locate the single ground fault can be summarized, which are:

i. The CM currents flowing through unhealthy feeder have the maximum value;

ii. The phase-to-ground fault has completely different waveforms in sub-bands from the pole-to-ground faults;

iii. The pole-to-ground faults happening in the Houses have different waveforms in 6^{th} and 7^{th} sub-bands from other kinds of ground faults;

iv. If the ground fault occurred after the Garages, depends on which one is the unhealthy feeder, the amplitudes of Igcm1 or Igcm2 would be much higher than the other one.

4.3 Location Algorithm

4.3.1 First Part of Location Algorithm

The flowchart of the location algorithm proposed in this thesis is shown in Figure 4-42. The first part of the location algorithm is finding out the category that the fault belongs to. The sensors start to collect the data of CM currents at 0.651s and continue to 0.72s. As what is shown in Figure 4-43, the time range of the first snapshot is from 0.651s to 0.668s, which includes the first cycle and the transient part of the whole signal. Based on the characteristics shown in Figure 4-39, the signal in the first snapshot can be used to find out if the single ground fault happens in Houses or not.

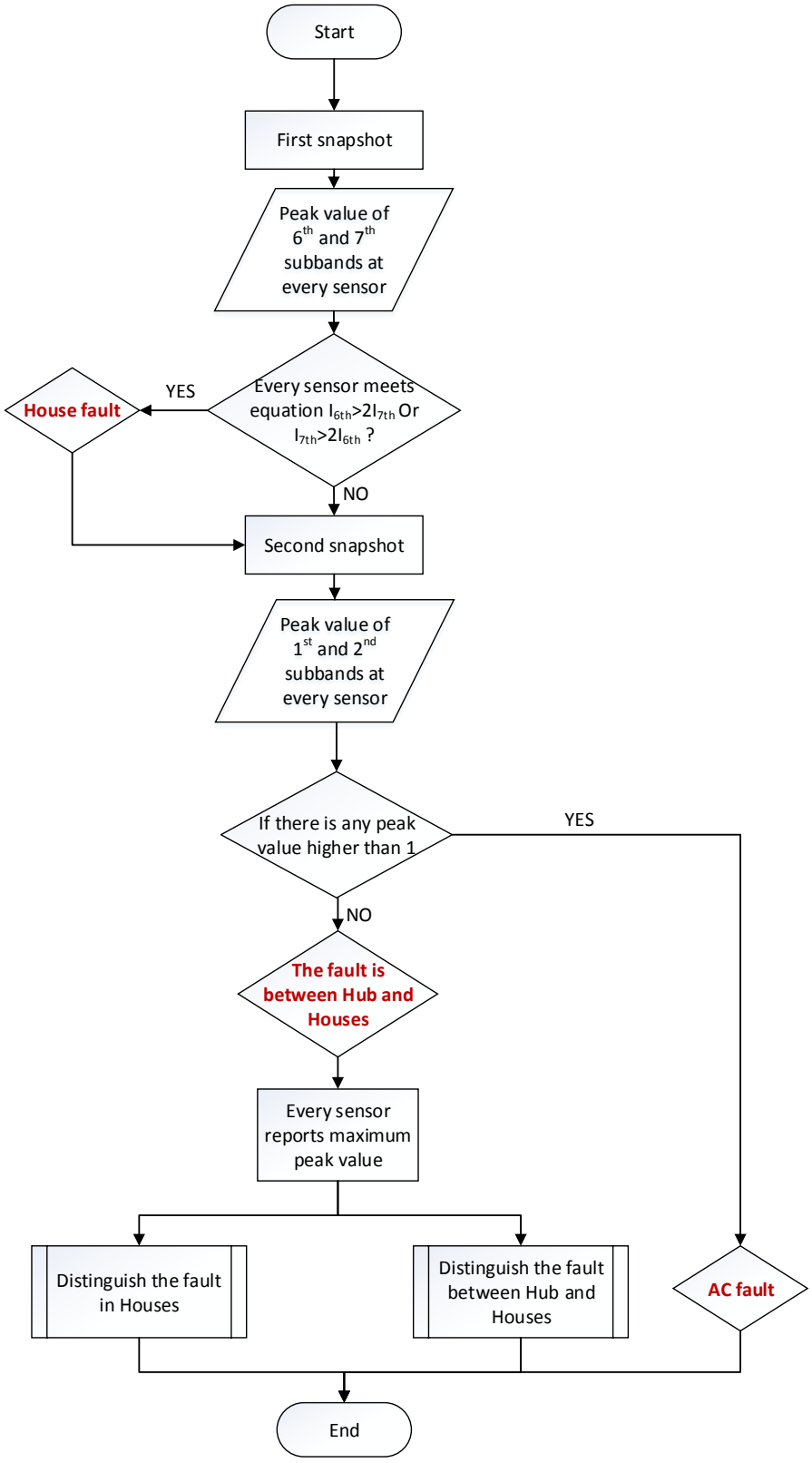

Figure 4-42 The flowchart of the location algorithm

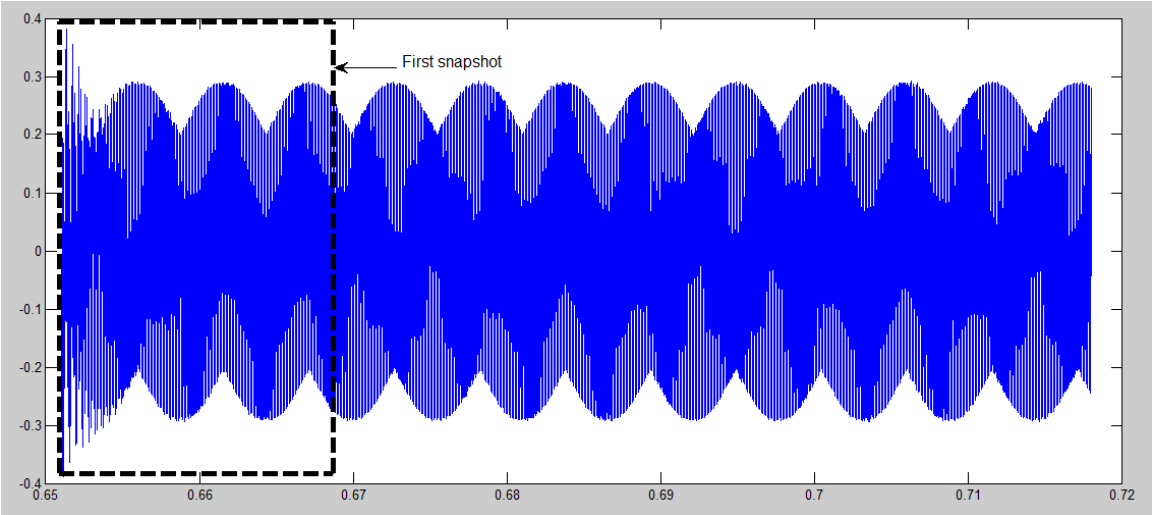

Figure 4-43 The definition of the first snapshot

To find out if the single ground fault is occurring in Houses, peak values of the 6th and 7th sub-bands of every CM current in DC system are required and listed in Table 4-9. From Table 4-9, it is noticed that if the ground fault was in Houses, there would be a big difference between the peak values of the 6th and 7th sub-bands of every CM current in DC system. And technically, the difference would be bigger than twice. Based on this difference, the rule that if every sensor could meet the equations that $I_{6th}>2I_{7th}$ or $I_{7th}>2I_{6th}$, then it is believed that the fault is in Houses is set up. And as what is highlighted in Table 4-9, GF1 and GF6 are not in the Houses because not all the sensors meet the equations.

Table 4-9 Peak values of the 6th and 7th sub-bands of every CM current in DC system

	GF1	**GF6**	**GF71**	**GF72**	**GF73**
Icm1_6	0.0343	0.002	0.1513	0.0124	0.0111
Icm1_7	0.0479	0.0035	0.0724	0.0819	0.0868
Icm2_6	0.0333	0.0082	0.0739	0.1952	0.0301
Icm2_7	0.0468	0.0165	0.0134	0.0492	0.0127
Icm3_6	0.1786	0.0047	0.0016	0.0015	0.0018

Icm3_7	0.1864	0.0096	0.0039	0.0026	0.0038
Igcm1_6	0.0343	0.002	0.0019	0.0028	0.0013
Igcm1_7	0.0479	0.0035	0.0045	0.0022	0.0029
Igcm2_6	0.0333	0.0082	0.002	0.0019	0.0025
Igcm2_7	0.0468	0.0165	0.0046	0.004	0.0062

After finding out if the single ground fault happens in Houses or not, the second snapshot of every signal will be taken. The time range of the second snapshot is from 0.668s to 0.702s including two cycles. Figure 4-44 shows how the second snapshot looks like.

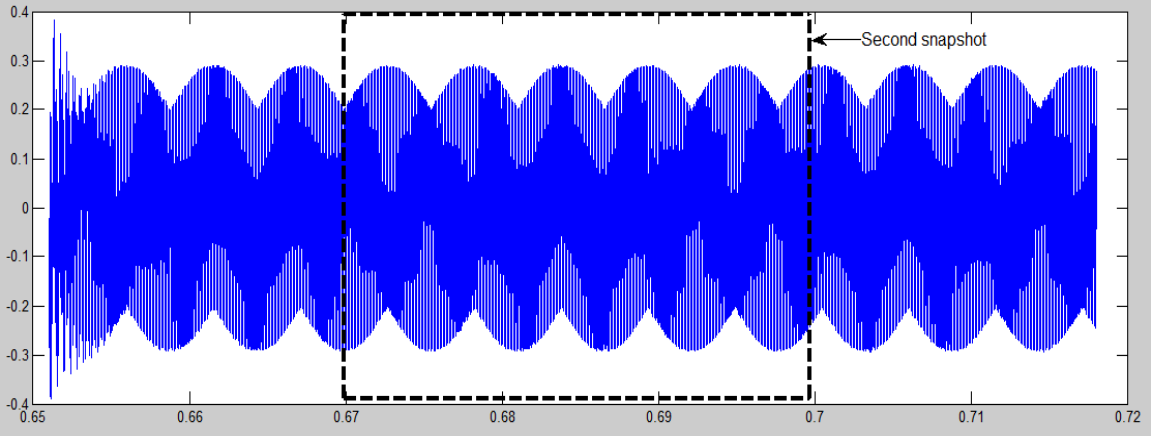

Figure 4-44 The definition of the second snapshot

Figure 4-45 shows the comparison result of the first two sub-bands of Icm1 of GF1 and GF2. The signal in the second snapshot is exactly the stable part of the signal. In this part, as what is shown in Figure 4-45 and what is pointed out in Section 4.2, the information in this snapshot can be used to find out if the fault is in AC system by comparing the waveform. And it also can be used to locate all kinds of the fault accurately by comparing the peak values. And in order to simplify the location algorithm, only the waveforms and data in the 1st and the 2nd sub-bands will be used.

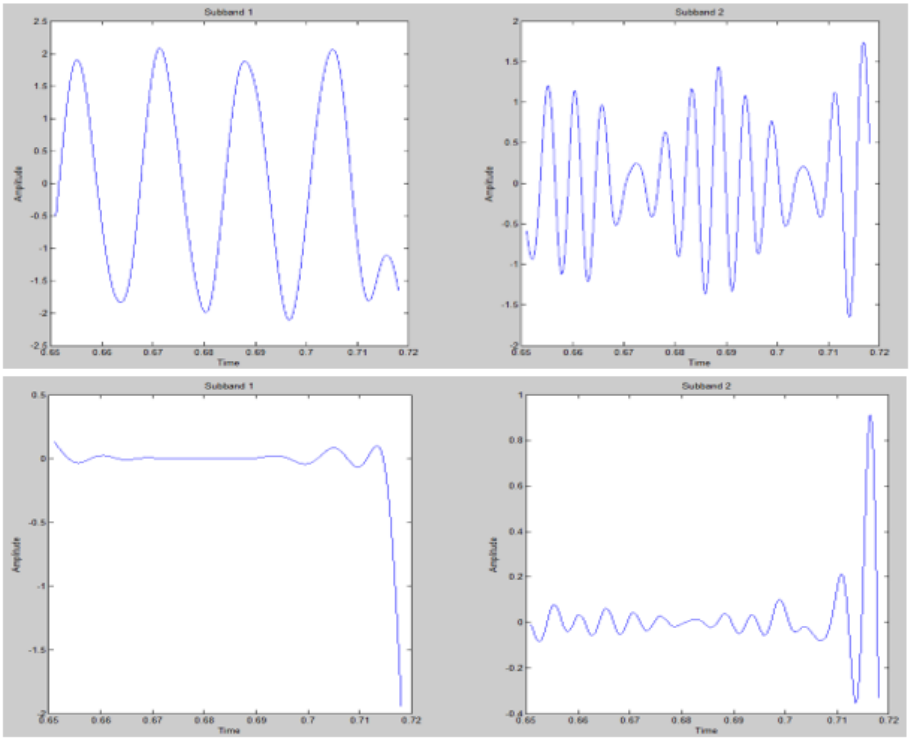

Figure 4-45 Comparison results of first two sub-bands of Icm1

Table 4-10 lists the peak values of the 1st and 2nd sub-bands of every CM current of GF1, GF3 and GF5. Based on Table 4-10, the rule that if there is one or more peak value which is higher than 1, then this fault is in AC system is set up.

Table 4-10 Peak values of the 1st and 2nd sub-bands of every CM current (GF1, GF3, GF5)

	GF1	GF3	GF5
AC_1	2.0859	0.0216	0.0228
AC_2	1.4371	0.1002	0.0998
Icm1_1	0.6686	0.0154	0.0116
Icm1_2	0.4509	0.0096	0.0298
Icm2_1	0.668	0.0119	0.0149
Icm2_2	0.4506	0.0308	0.0093
Icm3_1	0.4055	0.0029	0.003

Icm3_2	0.2694	0.011	0.0108
Igcm1_1	0.6686	0.0154	0.0116
Igcm1_2	0.4509	0.0096	0.0298
Igcm2_1	0.668	0.0152	0.0149
Igcm2_2	0.4506	0.0096	0.0093

4.3.2 Distinguish the faults between Hub and Houses

After finding out the category that the fault belongs to, it is time to locate the single ground fault accurately. The tool is still the peak values of 1st and 2nd sub-bands of every CM current. Based on the characteristics listed in Section 4.2.4, which are the CM currents flowing through unhealthy feeder have the maximum value and if the ground fault occurred after the Garages, depends on which one is the unhealthy feeder, the amplitudes of Igcm1 or Igcm2 would be much higher than the other one, a process of comparing the values is set up and its flowchart is shown in Figure 4-46 The flowchart of distinguishing the faults between Hub and Houses. Here is one thing needed to be explained, which is every CM current in DC system will report two peak values since both of the 1st and 2nd sub-bands are used. However, in order to reduce the error and improve the accuracy, eventually only the higher one will be reported and used to compare.

All the required peak values are listed in Table 4-11 Peak values of the 1st and 2nd sub-bands of every CM current (GF2 to GF6). All of the higher peak values have been highlighted in bold. Following the process of comparing, the values in red show the result of comparison, which meets the characteristic that the CM currents flowing through unhealthy feeder have the maximum value. And in order to tell if the fault happens after

the Garages or not, based on the characteristic that if the ground fault occurred after the Garages, the amplitudes of Igcm1 or Igcm2 would be much higher than the other one, the rule that if the equations that $|Icm2\text{-}Igcm2| > 0.1$ or $|Icm1\text{-}Igcm1| > 0.1$ can be met, then this fault is after the Garages is set up.

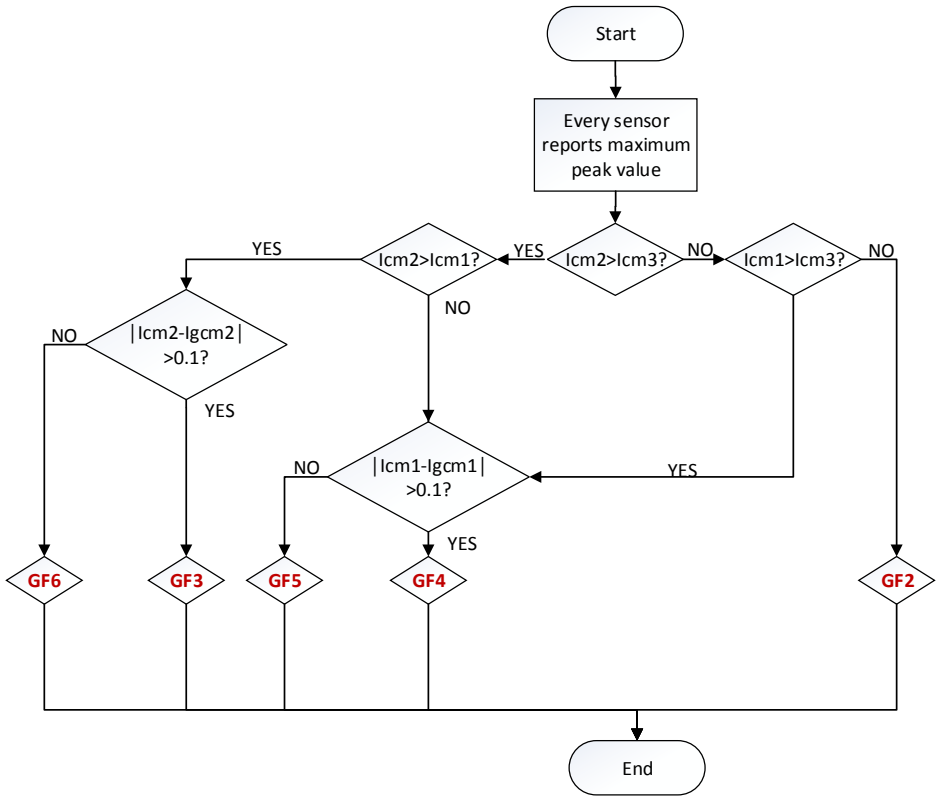

Figure 4-46 The flowchart of distinguishing the faults between Hub and Houses

Table 4-11 Peak values of the 1st and 2nd sub-bands of every CM current (GF2 to GF6)

	GF2	GF3	GF4	GF5	GF6
Icm1_1	0.0047	**0.0154**	**0.0443**	0.0116	0.0048
Icm1_2	**0.0103**	0.0096	0.0304	**0.0298**	**0.0106**
Icm2_1	0.0047	0.0119	0.0047	**0.0149**	**0.043**
Icm2_2	**0.0103**	**0.0308**	**0.0101**	0.0093	0.0308
Icm3_1	0.0291	0.0029	0.0048	0.003	0.005

Icm3_2	**0.0301**	**0.011**	**0.0235**	**0.0108**	**0.0237**
Igcm1_1	0.0047	**0.0154**	0.0048	0.0116	0.0048
Igcm1_2	**0.0103**	0.0096	**0.0102**	**0.0298**	**0.0106**
Igcm2_1	0.0047	**0.0152**	0.0047	**0.0149**	**0.043**
Igcm2_2	**0.0103**	0.0096	**0.0101**	0.0093	0.0308

4.3.3 Distinguish the faults in Houses

About finding out the house where the fault is, the same characteristics with what are mentioned in Section 4.3.2 are used as the tool. The flowchart of the process of comparing the values is shown in Figure 4-47 The flowchart of distinguishing the faults in Houses. Since there is no doubt that the fault occurring in Houses is after Garages, it is not necessary to compare Icm1, Icm2 and Icm3. And because there is no Garage in Feeder 3, Icm3 can be regarded as Igcm3 to get involved with the process. Thus, it is enough that only comparing Igcm1, Igcm2 and Icm3.

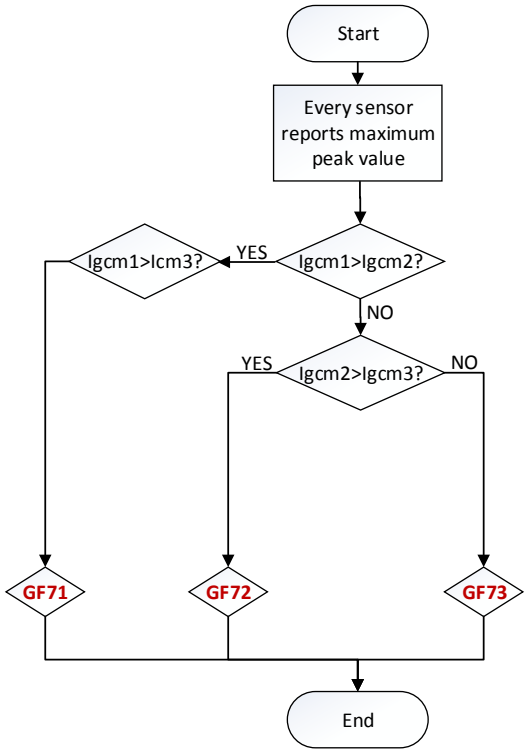

Figure 4-47 The flowchart of distinguishing the faults in Houses

Table 4-12 lists all of the required peak values. Still, the higher peak values have been highlighted in bold and red values are showing the result of comparison.

Table 4-12 Peak values of the 1st and 2nd sub-bands of three CM currents (GF71 to GF73)

	GF71	**GF72**	**GF73**
Icm3_1	0.0009	0.0001	**0.0026**
Icm3_2	**0.0011**	**0.0008**	0.0007
Igcm1_1	**0.0033**	0.0002	**0.0015**
Igcm1_2	0.0008	**0.0008**	0.0010
Igcm2_1	**0.0030**	**0.0023**	**0.0013**
Igcm2_2	0.0011	0.0011	0.0010

Chapter 5 Conclusion and Future Work

5.1 Conclusion

In this thesis, A DC microgrid is built and single ground fault at different locations is applied. To locate the ground fault accurately, WT is applied to decompose the CM currents caused by the fault and capture the characterization of different ground faults. Eventually, based on these characterizations, a location algorithm which can be used to locate the different kinds of ground fault in DC microgrid is proposed.

5.2 Future Work

In this thesis, the grounding resistance of single ground fault is fixed. Considering about the real situation of soil, it would be more practical if the grounding resistance was set up as variable. On the other hand, both of the different grounding types and if the PV panels make contributions to the ground fault would change the CM currents significantly and make it more complicated and difficult to locate the fault. Another important consideration is pratical implementation of the ground fault location algorithm. A sample frequency of 400kHz will drive cost into the system and may not be practically implementable. This sample frequency is driven mainly by the common mode switching frequency of the converters that are connected into the grid. The trade-offs between switching frequency and CM current sampling need to be explored. Given these factors, there is still a lot of work to do.

References

[1] Salonen, P., Kaipia, T., Nuutinen, P., Peltoniemi, P., & Partanen, J. (2008). An LVDC distribution system concept. In *Nordic Workshop on Power and Industrial Electronics (NORPIE/2008), June 9-11, 2008, Espoo, Finland*. Helsinki University of Technology.

[2] Hatziargyriou, N., Asano, H., Iravani, R., & Marnay, C. (2007). Microgrids.*IEEE power and energy magazine*, *5*(4), 78-94.

[3] Venkataramanan, G., & Illindala, M. (2002). Microgrids and sensitive loads. In *Power Engineering Society Winter Meeting, 2002. IEEE* (Vol. 1, pp. 315-322). IEEE.

[4] Salomonsson, D., Soder, L., & Sannino, A. (2009). Protection of low-voltage DC microgrids. *IEEE Transactions on Power Delivery*, *24*(3), 1045-1053.

[5] Das, R., & Kunsman, S. A. (2004, April). A novel approach for ground fault detection. In *Protective Relay Engineers, 2004 57th Annual Conference for*(pp. 97-109). IEEE.

[6] Zhongjian, K., Ruiying, L., & Yang, C. (2015, May). A fault location method for single-phase grounding fault in distribution network. In *The 27th Chinese Control and Decision Conference (2015 CCDC)* (pp. 5534-5539). IEEE.

[7] Sarma, P., Nirmala, S. R., & Sarma, K. K. (2014, February). ECG classification using wavelet subband energy based features. In *Signal Processing and Integrated Networks (SPIN), 2014 International Conference on* (pp. 785-790). IEEE.

[8] Zhang, Z., Li, A., Liu, Y., & Shen, Y. (2008, June). Detection of small current grounding fault line based on wavelet and neural networks. In*Intelligent Control and Automation, 2008. WCICA 2008. 7th World Congress on* (pp. 5258-5262). IEEE.

[9] Wang, M., & Stathaki, T. (2008, August). Cable fault recognition using multiple wavelet neural networks. In *2008 International Conference on Wavelet Analysis and Pattern Recognition* (Vol. 1, pp. 221-226). IEEE.

[10] Li, W., Monti, A., & Ponci, F. (2014). Fault detection and classification in medium voltage DC shipboard power systems with wavelets and artificial neural networks. *IEEE Transactions on Instrumentation and Measurement*,*63*(11), 2651-2665.

[11] Zhai, J., Ding, Y., Xu, B., & Li, Y. (2012, November). Wavelet and travelling wave based DC cable fault localization in MTDC. In *Environmental Electromagnetics (CEEM), 2012 6th Asia-Pacific Conference on* (pp. 206-209). IEEE.

[12] Jing, G., & Ru, L. (2009, November). A new wavelet packet method of single-phase earth fault line selection in distribution network based on the maximum difference comparison. In *Electrical Machines and Systems, 2009. ICEMS 2009. International Conference on* (pp. 1-5). IEEE.

[13] Wang, S., Bi, T., & Jia, K. (2015, July). Wavelet entropy based fault detection approach for MMC-HVDC lines. In *2015 IEEE Power & Energy Society General Meeting* (pp. 1-5). IEEE.

[14] He, Z., Fu, L., Lin, S., & Bo, Z. (2010). Fault detection and classification in EHV transmission line based on wavelet singular entropy. *IEEE transactions on Power Delivery*, *25*(4), 2156-2163.

[15] Allipilli, Y., & Rao, G. N. (2015, January). Detection and classification of faults in transmission lines based on wavelets. In *Electrical, Electronics, Signals, Communication and Optimization (EESCO), 2015 International Conference on* (pp. 1-6). IEEE.

[16] De Kerf, K., Srivastava, K., Reza, M., Bekaert, D., Cole, S., Van Hertem, D., & Belmans, R. (2011). Wavelet-based protection strategy for DC faults in multi-terminal VSC HVDC systems. *IET Generation, Transmission & Distribution*, *5*(4), 496-503.

[17] Wang, Z., & Balog, R. S. (2015). Arc Fault and Flash Signal Analysis in DC Distribution Systems Using Wavelet Transformation. *IEEE Transactions on Smart Grid*, *6*(4), 1955-1963.

[18] Xiangjun, Z., Li, K. K., & Chan, W. L. (2002, October). Wavelet analysis based protection for high impedance ground fault in supply systems. In*Power System Technology, 2002. Proceedings. PowerCon 2002. International Conference on* (Vol. 1, pp. 275-279). IEEE.

[19] R. M. Cuzner, K. Palaniappan and Z. J. Shen, "System specification for a DC community microgrid and living laboratory embedded in an urban environment," 2015 International Conference on Renewable Energy Research and Applications (ICRERA), Palermo, 2015, pp. 1119-1125

[20] Cuzner, R. M., Sielicki, T., Archibald, A. E., & McFarlin, D. A. (2011, April). Management of ground faults in an ungrounded multi-terminal zonal DC distribution system with auctioneered loads. In *2011 IEEE Electric Ship Technologies Symposium* (pp. 300-305). IEEE.

[21] Carminati, M., Grillo, S., Piegari, L., Ragaini, E., & Tironi, E. (2015, June). Fault protection analysis in low voltage DC microgrids with PV generators. In*Clean Electrical Power (ICCEP), 2015 International Conference on* (pp. 184-191). IEEE.

[22] Brovont, A. D., & Pekarek, S. D. (2015, June). Equivalent circuits for common-mode analysis of naval power systems. In *Electric Ship Technologies Symposium (ESTS), 2015 IEEE* (pp. 245-250). IEEE.

[23] Zhou, L., Wang, L., Wu, Z., Wang, G., & Wu, M. (2015, October). Reduction of common-mode current in parallel connected PV-inverters with negative grounding. In *Electrical Machines and Systems (ICEMS), 2015 18th International Conference on* (pp. 1660-1665). IEEE.

[24] Song, X., Chen, W., Xuan, Y., Zhang, B., & Zhang, J. (2015, June). Common mode leakage current analysis for transformerless PV system with long DC side cables. In *2015 9th International Conference on Power Electronics and ECCE Asia (ICPE-ECCE Asia)* (pp. 2475-2480). IEEE.

[25] Walnut, D. F. (2013). *An introduction to wavelet analysis*. Springer Science & Business Media.

[26] Santoso, S., Powers, E. J., Grady, W. M., & Hofmann, P. (1996). Power quality assessment via wavelet transform analysis. *IEEE transactions on Power Delivery*, *11*(2), 924-930.

[27] Robertson, D. C., Camps, O. I., Mayer, J. S., & Gish, W. B. (1996). Wavelets and electromagnetic power system transients. *IEEE Transactions on Power Delivery*, *11*(2), 1050-1058.

[28] Zhang, J. Y., Cui, L. L., Yao, G. Y., & Gao, L. X. (2007, November). Research on the selection of wavelet function for the feature extraction of shock fault in the bearing diagnosis. In *2007 International Conference on Wavelet Analysis and Pattern Recognition* (Vol. 4, pp. 1630-1634). IEEE.

[29] Chun-Lin, L. (2010). A tutorial of the wavelet transform. *NTUEE, Taiwan*.

[30] Antonino-Daviu, J., Riera-Guasp, M., Roger-Folch, J., Martínez-Giménez, F., & Peris, A. (2006). Application and optimization of the discrete wavelet transform for the detection of broken rotor bars in induction machines. *Applied and Computational Harmonic Analysis*, *21*(2), 268-279.